การวิเคราะห์หน่วยแรงทีทั่วไปสำหรับรอยร้าวในตัวกลางไพอิโซอิเล็กทริกเชิงเส้น
สามมิติภายใต้เงื่อนไขขอบเขตที่ผิวรอยร้าวแบบต่างๆโดยระเบียบวิธีบาวดารีเอลิเมนต์

นายวารุจ ลิ่มวิบูลย์

วิทยานิพนธ์นี้เป็นส่วนหนึ่งของการศึกษาตามหลักสูตรปริญญาวิศวกรรมศาสตรมหาบัณฑิต
สาขาวิชาวิศวกรรมโยธา ภาควิชาวิศวกรรมโยธา
คณะวิศวกรรมศาสตร์ จุฬาลงกรณ์มหาวิทยาลัย
ปีการศึกษา 2558

ANALYSIS OF GENERALIZED T-STRESS FOR CRACKS IN 3D LINEAR PIEZOELECTRIC MEDIA UNDER VARIOUS CRACK-FACE CONDITIONS BY BEM

Mr. Varuj Limwibul

A Thesis Submitted in Partial Fulfillment of the Requirements
for the Degree of Master of Engineering Program in Civil Engineering
Department of Civil Engineering
Faculty of Engineering
Chulalongkorn University
Academic Year 2015

Thesis Title	ANALYSIS OF GENERALIZED T-STRESS FOR CRACKS IN 3D LINEAR PIEZOELECTRIC MEDIA UNDER VARIOUS CRACK-FACE CONDITIONS BY BEM
By	Mr. Varuj Limwibul
Field of Study	Civil Engineering
Thesis Advisor	Associate ProfessorJaroon Rungamornrat, Ph.D.
Thesis Co-Advisor	Weeraporn Phongtinnaboot, Ph.D.

Accepted by the Faculty of Engineering, Chulalongkorn University in Partial Fulfillment of the Requirements for the Master's Degree

.....Dean of the Faculty of Engineering

(Associate ProfessorSupot Teachavorasinskun, D.Eng.)

THESIS COMMITTEE

.....Chairman

(ProfessorTeerapong Senjuntichai, Ph.D.)

.....Thesis Advisor

(Associate ProfessorJaroon Rungamornrat, Ph.D.)

.....Thesis Co-Advisor

(Weeraporn Phongtinnaboot, Ph.D.)

.....Examiner

(Associate ProfessorAkhrawat Lenwari, Ph.D.)

.....External Examiner

(Yasothorn Sapsathiarn, Ph.D.)

วารุจ ลิ่มวิบูลย์ : การวิเคราะห์หน่วยแรงทีทั่วไปสำหรับรอยร้าวในตัวกลางไพอิโซอิเล็กทริกเชิงเส้นสามมิติภายใต้เงื่อนไขขอบเขตที่ผิวรอยร้าวแบบต่างๆโดยระเบียบวิธีบาวดารีเอลิเมนต์ (ANALYSIS OF GENERALIZED T-STRESS FOR CRACKS IN 3D LINEAR PIEZOELECTRIC MEDIA UNDER VARIOUS CRACK-FACE CONDITIONS BY BEM) อ.ที่ปรึกษาวิทยานิพนธ์หลัก: รศ. ดร.จรูญ รุ่งอมรรัตน์, อ.ที่ปรึกษาวิทยานิพนธ์ร่วม: ดร.วีรพร พงศ์ติณบุตร, 67 หน้า.

วิทยานิพนธ์นี้นำเสนอระเบียบวิธีเชิงตัวเลขที่ถูกต้องและมีประสิทธิภาพสำหรับหาค่าหน่วยแรงทีทั่วไปของรอยร้าวในตัวกลางไพอิโซอิเล็กทริกเชิงเส้นไร้ขอบเขตสามมิติภายใต้เงื่อนไขที่ผิวรอยร้าวแบบต่างๆ สมการกำกับหลักถูกพัฒนาในรูปแบบของสมการเชิงปริพันธ์พื้นผิวคู่ที่เกี่ยวข้องกับข้อมูลที่ผิวรอยร้าวและเคอร์เนลเอกฐานต่ำเท่านั้น สมการปริพันธ์ทั้งสองสมการและเงื่อนไขที่ผิวรอยร้าวทั้งสี่แบบประกอบไปด้วยเงื่อนไขแบบซึมผ่านไม่ได้ แบบซึมผ่านได้ แบบซึมผ่านได้บางส่วน และแบบสอดคล้องเชิงพลังงาน ถูกนำมาใช้สร้างปัญหาค่าขอบเขตของตัวกลางไพอิโซอิเล็กทริกที่มีรอยร้าว สมการปริพันธ์สำหรับการกระโดดของแรงทั่วไปที่ผิวรอยร้าวร่วมกับเงื่อนไขที่ผิวรอยร้าวใช้สำหรับหาผลเฉลยของการกระโดดของการขจัดทั่วไปที่ผิวรอยร้าว ในขั้นตอนการหาผลเฉลย ระเบียบวิธีกาเลอคินบาวดารีเอลิเมนต์แบบสมมาตรเชิงเอกฐานต่ำและการประมาณแบบพิเศษที่บริเวณขอบรอยร้าวถูกนำมาใช้ในการประมาณผลเฉลย และระบบสมการพีชคณิตไร้เชิงเส้นในกรณีเงื่อนไขผิวรอยร้าวแบบซึมผ่านได้บางส่วนและแบบสอดคล้องเชิงพลังงานหาผลเฉลยโดยใช้อัลกอริทึมมาตรฐานของนิวตัน-ราฟสัน เมื่อหาค่าการกระโดดของการขจัดทั่วไปที่ผิวรอยร้าวได้แล้ว ค่าผลรวมของการขจัดทั่วไปที่ผิวรอยร้าวสามารถหาได้จากสมการปริพันธ์ที่เหลือโดยใช้ระเบียบวิธีมาตรฐานของกาเลอคิน ข้อมูลที่ได้นี้ถูกนำไปใช้ในการหาค่าหน่วยแรงทีทั่วไปที่ขอบรอยร้าว ผลที่ได้จากการทดลองเชิงตัวเลขแสดงให้เห็นว่าระเบียบวิธีที่นำเสนอให้ผลเฉลยเชิงตัวเลขที่มีความถูกต้องสูงและมีประสิทธิภาพในเชิงคำนวณ นอกจากนี้ค่าหน่วยแรงทีทั่วไปที่ทำนายได้ยังขึ้นอยู่กับเงื่อนไขที่ผิวรอยร้าวที่ใช้ในการจำลองอย่างมีนัยสำคัญ

ภาควิชา วิศวกรรมโยธา ลายมือชื่อนิสิต .....

สาขาวิชา วิศวกรรมโยธา ลายมือชื่อ อ.ที่ปรึกษาหลัก .....

ปีการศึกษา 2558 ลายมือชื่อ อ.ที่ปรึกษาร่วม .....

5770300821 : MAJOR CIVIL ENGINEERING
KEYWORDS: CRACK-FACE CONDITIONS / CRACKS / GENERALIZED T-STRESS / PIEZOELECTRIC MEDIA / BOUNDARY INTEGRAL EQUATIONS

VARUJ LIMWIBUL: ANALYSIS OF GENERALIZED T-STRESS FOR CRACKS IN 3D LINEAR PIEZOELECTRIC MEDIA UNDER VARIOUS CRACK-FACE CONDITIONS BY BEM. ADVISOR: ASSOC. PROF.JAROON RUNGAMORNRAT, Ph.D., CO-ADVISOR: WEERAPORN PHONGTINNABOOT, Ph.D., 67 pp.

This thesis presents an efficient and accurate numerical procedure for the determination of the generalized T-stress components of cracks in a three-dimensional, linear piezoelectric, infinite medium under various crack-face conditions. The key formulation is established in terms of dual weak-form boundary integral equations involving only the crack-face data and weakly singular kernels. This pair of integral equations is then integrated with one of the four crack-face conditions including impermeable, permeable, semi-permeable and energetically consistent conditions to form the complete boundary value problem for a piezoelectric cracked medium. The boundary integral equation for the jump in the crack-face generalized traction coupled with the crack-face condition is solved first for the jump in the crack-face generalized displacement. In the solution procedure, a weakly singular symmetric Galerkin boundary element method and the special near-front approximation are adopted in the discretization whereas a system of nonlinear algebraic equations arising from the semi-permeable and energetically consistent crack-face conditions is solved by standard Newton-Raphson algorithm. Once the jump in the crack-face generalized displacement is completely determined, the sum of the crack-face generalized displacement is then obtained by solving the remaining integral equation via a standard Galerkin technique. This solved crack-face data is then employed to directly extract the generalized T-stress components along the crack front. Results from numerical experiments of various scenarios indicate that the proposed technique yields highly accurate numerical solutions and is computationally robust. In addition, the predicted generalized T-stresses are significantly influenced by the crack-face condition adopted in the modeling.

Department:	Civil Engineering	Student's Signature	.....
Field of Study:	Civil Engineering	Advisor's Signature	.....
Academic Year:	2015	Co-Advisor's Signature	.....

ACKNOWLEDGEMENTS

Firstly, my deepest gratitude is to my thesis advisor, Assoc. Prof. Dr. Jaroon Rungamornrat who has been an amazing support throughout my work since my senior project in my Bachelor's degree. His patience and support helped me overcome many crisis situations and steered me in the right direction until my thesis is completed. Secondly, my co-advisor, Dr. Weeraporn Phontinnaboot has been always there to listen and give advice. I am deeply grateful to him for the long discussions that helped me sort out the technical details of my work. I also want to thank all the previous thesis from my seniors for their dedication to their thesis and allowing me to use their works as a reference and information towards the study of my thesis. Many friends have helped me stay sane through these difficult years. Their support and care helped me overcome setbacks and stay focused on my graduate study. I greatly value their friendship and I deeply appreciate their belief in me. Most importantly, thank you for the love and patience of my family. My immediate family to whom this dissertation is dedicated to, has been a constant source of love, concern, support and strength all these years. I would like to express my heart-felt gratitude to my family. Also, I warmly appreciate my second-reader whom have encouraged the correct use of grammar and punctuations and for carefully reading and commenting on countless revisions of this manuscript. Finally, all of this work would not have been possible without the financial support from the Faculty of Engineering, Chulalongkorn University that awarded the scholarship for me to pursue my thesis and master's degree.

CONTENTS

Page

Page

Page

LIST OF TABLES

LIST OF FIGURES

Page

Page

Page

Page

LIST OF ABBREVIATIONS

C_{mJ}^{tK}	weakly singular kernel appearing in boundary integral equation
D_i	components of electric induction
E_i	components of electric field
E_{iJKm}	generalized moduli
e_{mij}	piezoelectric constants
G_{tK}^{J}	weakly singular kernel appearing in boundary integral equation
H_{tK}^{J}	weakly singular kernel appearing in boundary integral equation
n_i	components of unit normal vector
S_{iJ}^{P}	generalized stress fundamental solution
S_c^+, S_c^-	upper and lower crack surfaces
t_J	components of generalized traction
t_j	components of mechanical traction
U_J^P	generalized displacement fundamental solution
u_j	components of displacement
u_K	components of generalized displacement
$\boldsymbol{x}$	interior point of body
$\boldsymbol{z}$	unit vector normal to position vector $\boldsymbol{\xi} - \boldsymbol{x}$
δ_{IJ}	standard Kronecker-delta symbol
ε_{ij}	components of strain tensor
ε_{ijk}	standard alternating symbol
ϕ	electric potential
κ_{im}	dielectric permittivities
σ_{ij}	components of stress tensor
$\boldsymbol{\xi}$	point on the crack surface

CHAPTER 1
INTRODUCTION

This chapter presents the key motivation and significance of the present study and then provides a summary resulting from an extensive review of background and advances in the modeling and analysis of fractures in piezoelectric media. Next, the main objectives, scope of work, methodology, and research procedure are briefly summarized. Finally, the expected outcome and contribution of the present work is addressed.

1.1 MOTIVATION AND SIGNIFICANCE

Nowadays, applications of piezoelectric materials have been increasingly found in many disciplines including industries and engineering field due to their strong electro-mechanical coupling effects. These materials have been found in many parts and components of modern tools and devices such as sensors and actuators (e.g., sonar, ultra-precision positioner, ultrasonic cleaner, ink jet print head, etc.) and transmitters (e.g., remote control of vehicles and cellular phones) (see for examples, Birman et al., 1999; Cai et al., 2001; Denda and Mansukh, 2005). Besides their attractive/desirable characteristics, it has been also known that most of available piezoelectric materials possess brittle failure mechanism and are exposed to fractures since they have relatively low fracture toughness. This, as a result, renders components, devices and tools made from this class of smart materials prone to fracture-induced damages/failures during their applications. Analysis, assessment, and design to avoid such undesirable failures are therefore essential and this obviously necessitates extensive investigations to understand fundamental fracture behavior and related damage/failure mechanisms of piezoelectric materials.

Two well-known approaches, namely the experimental investigations and mathematical simulations, have been widely employed to explore the fundamental fracture characteristics of piezoelectric solids (e.g., Shindo et al., 2007; Okayasu et al. , 2010; Lee et al., 2011). Although results obtained from the first group can yield reliable information reflecting the real response and behavior, such findings are highly

dependent on testing parameters/environments controlled in laboratories and, in addition, costs associated with testing equipment, materials, and preparing of specimens can be very demanding. Therefore, applications of those experimental observations to different/practical/large-scale scenarios can be quite limited. As the direct consequence, the mathematical modeling and simulations have become an attractive alternative and have been extensively utilized together with the proper governing physics and a set of basic experiments essential for modeling calibrations, to examine the fracture phenomena in piezoelectric media.

Mathematical models based upon a classical theory of linear piezoelectricity and linear fracture mechanics have been found well-suited and adequate for the physical simulations with a wide range of practical situations (see, for examples, the work of Pan (1999), Xu and Rajapakse (2001), Sanz et al. (2005), Wippler and Kuna (2007), Rungamornrat and Mear (2008a), Solis et al. (2009), and Rungamornrat et al. (2015)). However, most of previous studies have focused primarily on electric and stress intensity factors, which are essential fracture parameters completely characterizing the first singular part of an asymptotic near-front expansion of the electric induction and stress fields. As being well recognized, these parameters have been often utilized in the simulations of crack initiation and the path of crack advances. Recently, an important issue related to the role of the non-singular part in the near-front expansion, especially a constant term representing the uniform generalized stress acting along the crack plane (generally termed a generalized T-stress), on the fracture behavior of piezoelectric media arises. Several investigators, who studied the influence of T-stress on the near-front characteristics of cracks in a linearly elastic medium, pointed out that the T-stress strongly influences the shape and size of a plastic zone embedding the crack front (e.g., Larsson and Carlsson, 1973; Rice, 1974; Ueda et al., 1983, Du and Hancock, 1991), the hydrostatic tri-axiality of the stress field ahead of the crack boundary (e.g., Bilby et al., 1986; Du and Hancock, 1991), the fracture toughness (e.g., Williams and Ewing, 1972; Hancock et al., 1993; Ayatollahi et al., 1998; Smith et al., 2001; Tvergaard, 2008) and the direction of crack advances (e.g., Cotterell, 1966; Williams and Ewing, 1972; Ueda et al., 1983). Those findings have confirmed that ignorance of the T-stress data (i.e., the non-singular, constant term in the near-front

expansion) in the modeling can lead to inaccurate results or potentially mislead the conclusion. It is, therefore, essential to integrate the T-stress data in the fracture modeling and simulations and, as a result, the precise determination of such essential fracture information is a prerequisite.

Techniques based upon boundary integral equations are among numerical procedures that have been proven accurate and computationally efficient for modeling cracks in linear homogeneous media. A positive feature of this group of methods (over many domain-based approaches such as finite difference, finite element, and finite volume methods) is that the key governing equations contain only unknowns on the domain boundary and the surface of discontinuities and, as a result, the discretization of the boundary is only required instead of the whole domain. This apparently eases both the solution approximation and the generation/adaptation of meshes. These positive features, therefore, render the boundary-based methods efficient and attractive for analysis of linear fracture problems. While applications of this group of techniques to the linear piezoelectric fracture modeling has been recognized in the literature for the past three decades, existing techniques still have limited capabilities in the analysis for the generalized T-stress and it is required further investigations.

1.2 BACKGROUND AND REVIEW

Mathematical modeling of piezoelectric materials is a challenging task since this solid exhibits strong coupling between electrical and mechanical fields as well as their anisotropic behavior. Furthermore, the complexity of problems can significantly increase when the surface of displacement discontinuities such as dislocations and cracks are additionally present within the medium. In particular, the mechanical and electrical fields estimated by the classical linear theory of piezoelectricity become infinite along the boundary of discontinuities and also exhibit the rapid variation in a region embedding the discontinuities.

While various analytical techniques have been proposed to study fractures in linear piezoelectric media, most of existing investigations are limited only to simple

scenarios, such as simple crack geometries, simple loading conditions, and an infinite medium, due to the nature of the solution procedure (e.g., Park and Sun, 1995; Xu and Rajapakse, 1999; Chen and Shioya, 1999; Chen and Shioya, 2000; Chen et al., 2000; Xu and Rajapakse, 2001; Wang and Jiang, 2002; Wang and Mai, 2003; Li and Lee, 2004; Chen and Lim, 2005; Chiang and Weng, 2007; Li et al., 2011). To overcome the limitation of the analytical techniques and due to the increasing need to model complex and large-scale fracture problems, numerical techniques have been continuously established and become an attractive alternative as a result of their vast features and potential capability to treat problems within general settings (e.g., Pan, 1999; Rajapakse and Xu; 2001; Davi and Milazzo, 2001; Chen, 2003; Zhao et al., 2004; Sanz et al., 2005; Groh and Kuna, 2005; Rungamornrat and Mear, 2008; Wippler and Kuna, 2007; Qin et al., 2007; Solis et al., 2009; Phongtinnaboot et al., 2011).

Nevertheless, most of existing analytical, semi-analytical, and numerical procedures established for performing the analysis of linear piezoelectric fracture problems have focused mainly on the calculation of electric and stress intensity factors (see an extensive review of relevant studies in the work of Rungamornrat and Mear, 2008a; Phongtinnaboot, 2011; Phongtinnaboot et al., 2011; Rungamornrat et al., 2015). Relatively few studies concerning the generalized T-stress have been found and, unfortunately, most of them have restricted to two-dimensional boundary value problems (e.g., Zhu and Yang, 1999; Hao and Biao, 2004; Zhong and Li, 2008; Viola et al. , 2008; Liu et al., 2012). In particular, Zhu and Yang (1999) applied Stroh formalism together with the dislocation theory to obtain the generalized T-stress of an impermeable straight crack in a two-dimensional, homogeneous, linear piezoelectric infinite body under remote mechanical and electrical loading conditions. They also concluded that the generalized T-stress significantly affects the crack-kinking angle. Later, Hao and Biao (2004) used the principle of superposition and the Plemelj formulation to derive an analytical solution of the generalized T-stress for an impermeable straight crack embedded in a transversely isotropic, linear piezoelectric unbounded domain subjected to the uniform remote mechanical and electrical loading conditions. Results from their study indicated that the generalized T-stress depends strongly on both elastic and electric material constants. Later, Zhong and Li

(2008) reported the exact solution of the generalized T-stress for a semi-permeable Griffith crack in two-dimensional, transversely isotropic, linear piezoelectric solids with the influence of the magnetic field. In the analysis, a conventional method of Fourier transform was employed, and they found that the generalized T-stress in this coupling media is significantly different from that of the elastic material. In the same year, Viola et al. (2008) developed an analytical technique to investigate the contribution of non-singular terms on the electro-mechanical fields of a Griffith crack in two-dimensional, transversely isotropic, linear piezoelectric, unbounded media under uniform remote loading for three different types of crack-face conditions (i.e., electrically permeable, impermeable, and semi-permeable conditions). They concluded in this study that the non-singular terms, induced by the biaxial loading, has the considerable influence on the hoop stress, the elastic and electric displacements, and the stress components collinear to the crack. In addition, it was also pointed out that ignorance of the non-singular terms can mislead the prediction of the propagation direction since the influence of the bi-axiality of the applied load is neglected. Recently, Liu et al. (2012) employed a complex potential theory to construct the analytical solutions of both electric and elastic fields of an elliptical hole in a two-dimensional, transversely isotropic, linear piezoelectric infinite medium under the permeable condition, the uniform internal pressure, and the remote electro-mechanical loadings. Results for the limiting case, i.e., a straight crack, were also obtained. By comparing the obtained results with those from the work of Viola et al. (2008), it was confirmed that the non-singular terms play a crucial role on behavior of the near-front stress and electric induction.

Most recently, Subsathaphol (2013) and Subsathaphol et al. (2014) successfully developed a computational technique based on the weakly singular, boundary integral equation method and standard Galerkin procedure to calculate the generalized T-stress components of arbitrarily-shaped cracks in a three-dimensional, anisotropic, linear piezoelectric, whole space. While their proposed technique has been found computationally efficient and yielded highly accurate numerical solutions, their work is still restricted to cracks under electrically impermeable boundary conditions. The development based only on the impermeable crack-face condition, which is one of

several types of electrical boundary conditions commonly employed in simulations of cracks in piezoelectric media (see extensive review in the work of Rungamornrat et al., 2015) poses the major limitation of the modeling capability. As pointed out by several investigators such as Dunn (1994), Sosa and Khutoryansky (1996), Gao and Fan (1999), McMeeking (2001) and Ou and Chen (2003), the impermeable crack-face model is not appropriate for simulating actual cracks and may lead to inaccurate and erroneous prediction of the near-front electric/mechanical fields.

On the basis of an extensive literature review, the development of numerical techniques for calculating the generalized T-stresses of general cracks in a three-dimensional, linear piezoelectric body capable of treating several types of crack-face conditions such as electrically permeable, electrically impermeable, electrically semi-permeable, and energetically consistent crack-face conditions has not been found at least in the context of the fracture analysis by boundary integral equation methods. This significant gap of knowledge requires further investigations and it motivates the present study.

1.3 OBJECTIVES

The main aims of this study are (i) to establish an accurate and efficient numerical procedure based upon the weakly singular boundary integral equation method for determining the generalized T-stress components of cracks in three-dimensional piezoelectric media subjected to different types of crack-face conditions and (ii) to investigate the accuracy, convergence, and capability of the developed technique.

1.4 SCOPE OF RESEARCH

The present study is limited to (i) a three-dimensional infinite medium that is made from homogeneous, anisotropic, linear piezoelectric materials and free of the body electrical charge and body force, (ii) a body subjected to uniform remote electrical/mechanical loadings and arbitrarily distributed prescribed crack-face generalized tractions, (iii) a piecewise smooth crack surface, and (iv) a crack subjected

to either electrically permeable, electrically permeable, electrically semi-permeable, or energetically consistent crack-face conditions.

1.5 METHODOLOGY AND PROCEDURE

The present study mainly involves the development of a computational technique, based upon a regularized boundary element method and standard Galerkin technique for modeling fractures in linear piezoelectric media under different crack-face conditions. Three main tasks including the formulation of governing equations, the numerical implementations, and verification of the developed technique with various benchmark cases are carried out. Fundamental theories, key assumptions, research methodology, and research procedures employed in the current investigation are described as follows:

1) Basic field equations (e.g., conservation laws, constitutive laws, and kinematics) follow a classical theory of linear piezoelectricity.
2) Four different crack-face models (i.e., electrically permeable, electrically impermeable, electrically semi-permeable, and energetically consistent conditions) are employed to simulate the crack-face condition.
3) A set of standard boundary integral relations for both the generalized stresses and generalized displacements, resulting from the generalization of Somigliana's identity, is utilized in the formulation of governing integral equations.
4) A systematic regularization procedure suggested by Rungamornrat and Mear (2008b) is applied to obtain a set of singularity-reduced boundary integral relations/equations for cracks in anisotropic, linear piezoelectric, whole space without remote loadings.
5) The influence of remote electrical/mechanical loadings is incorporated into the formulation by using a superposition technique.
6) A system of completely regularized integral equations governing the unknown jump in and sum of the crack-face generalized displacements is formulated using results obtained from 4).

7) A weakly singular boundary element method is implemented to solve the governing boundary integral equation for the jump in the crack-face generalized traction to obtain the unknown jump in the crack-face generalized displacements. To enhance the accuracy of the near-front approximation, special interpolation functions proposed by Rungamornrat and Mear (2008a, b) are utilized to approximate the jump in the crack-face generalized displacements in the local region adjacent to the crack front.
8) A discretized system of linear equations obtained from the approximation of the boundary integral equation for the jump in the crack-face generalized tractions is sufficient for solving the unknown jump in the crack-face generalized displacements along the crack front for both impermeable and permeable cracks. For semi-permeable and energetically consistent cracks, additional nonlinear equations are obtained by weakly enforcing the crack-face conditions using a standard weighted residual technique. The combined system of linear and nonlinear algebraic equations is then solved by Newton-Raphson iterative scheme.
9) Once the jump in the crack-face generalized displacements and other involved unknowns are obtained for any type of crack-face conditions, the sum of the generalized displacements is then obtained by solving the weakly singular, weak-form generalized displacement boundary integral equation via a standard Galerkin procedure.
10) An explicit formula for computing the generalized T-stress under four types of crack-face conditions is established in terms of the gradient of the sum of the crack-face generalized displacement along the crack front.
11) An in-house computer code is implemented to compute the generalized T-stress of general cracks in three-dimensional, linear piezoelectric, whole space.
12) An implemented computer code is verified by benchmarking computed numerical results with available analytical and reliable reference solutions.

1.6 EXPECTED OUTCOME AND CONTRIBUTION

The proposed investigation offers an accurate and efficient computational procedure that is capable of calculating the generalized T-stress of general cracks in a three-dimensional, fully anisotropic, linear piezoelectric, unbounded medium under various crack-face conditions. The proposed technique has been developed in a general framework allowing the treatment of general crack geometry, material anisotropy, and loading and boundary conditions. The technique with such vast features should be potentially useful as a simulation tool for the modeling of crack advances with growth laws integrating the influence of non-singular terms. In addition, this present research should also provide a fundamental basis for the possible extension of existing computational techniques to model more complex problems such as cracks embedded in a body of finite dimensions or a body made of coupled/multi-field materials.

CHAPTER 2
PROBLEM FORMULATION

This chapter briefly summarizes basic field equations obtained from the classical theory of linear piezoelectricity, different types of crack-face boundary conditions, the clear description of a boundary value problem, and the development of singularity-reduced boundary integral equations governing unknown data on the crack surface.

2.1 BASIC FIELD EQUATIONS

From a classical theory of linear piezoelectricity, laws of conservation, kinematics, and constitutive relations governing all field quantities can be expressed in following forms

$$\sigma_{ij,i} = 0 \; ; \; D_{i,j} = 0 \tag{2.1}$$

$$\varepsilon_{ij} = \frac{1}{2}\left(u_{i,j} + u_{j,i}\right) \; ; \; E_i = -\phi_{,i} \tag{2.2}$$

$$\sigma_{ij} = E_{ijkm}\varepsilon_{km} - e_{mij}E_m \; ; \; D_i = e_{ikm}\varepsilon_{km} + \kappa_{im}E_m \tag{2.3}$$

where u_i, σ_{ij} and ε_{ij} represent components of the displacement vector, the stress tensor, and the strain tensor, respectively; ϕ, D_i and E_i denote the electric potential, components of the electrical induction vector, and components of the electrical field, respectively; E_{ijkm}, κ_{im} and e_{mij} denote elastic moduli, dielectric permittivity and piezoelectric constants of the medium, respectively; a notation $f_{,i}$ stands for $\partial f / \partial x_i$; and a standard rule for an indicial notation applies throughout (i.e., any lower-case index takes the values 1, 2, 3 and repeated or dummy indices indicate the summation over their range). For brevity in the presentation of all involved equations and the development presented further below, above field equations are rewritten in a more concise form, following the work of Rungamornrat and Mear (2008), as

$$\sigma_{iJ,i} = 0 \tag{2.4}$$

$$\sigma_{iJ} = E_{iJKm}u_{K,m} \tag{2.5}$$

where any lower case index still follow the same rules described above; any upper-case index takes the value 1, 2, 3 and 4 and any repeated or dummy upper-case index indicates the summation over its range; σ_{iJ} are termed components of the generalized stress which combine components of the stress tensor σ_{ij} and components of the electrical induction vector D_i by setting $\sigma_{i4} = D_i$; u_K are termed components of the generalized displacement which combine components of the displacement vector u_j and the electrical potential ϕ by setting $u_4 = \phi$; and E_{iJKm} are termed components of the generalized moduli that combines the elastic constants E_{ijkm}, the piezoelectric constants e_{mij} by setting $E_{ij4m} = E_{m4ji} = e_{mij}$, and the dielectric permittivity $E_{i44m} = E_{m44i} = -\kappa_{im}$. It is remarked that the constitutive relation in terms of gradients of the generalized displacement (2.5) can be readily obtained by simply substituting (2.2) into (2.3). Similarly, the generalized surface traction at any point on the smooth surface, with its components denoted by t_J, is defined by $t_J = \sigma_{iJ} n_i$ where n_i denote the components of an outward unit normal vector to the surface. More specifically, the generalized surface traction t_J combines components of the mechanical traction $t_j = \sigma_{ij} n_i$ and the surface electric charge $t_4 = \sigma_{i4} n_i = D_i n_i$.

2.2 PROBLEM DESCRIPTION

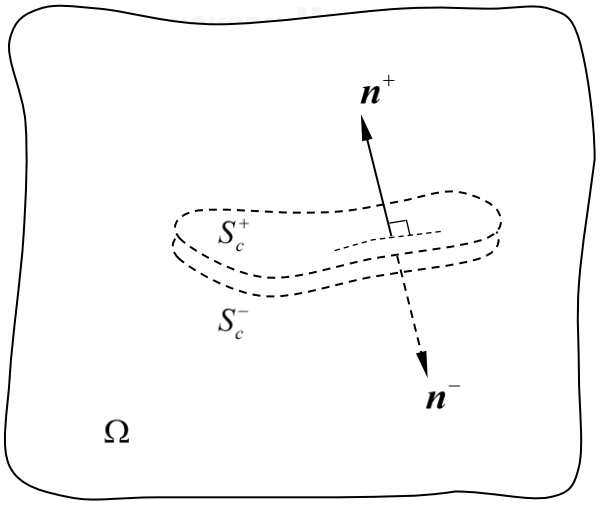

Figure 2.1 Schematic of isolated crack in homogeneous, anisotropic, linear piezoelectric whole space

Let us consider an isolated crack of arbitrary shape embedded in a whole space Ω as illustrated in Figure 2.1. A piezoelectric material constituting the body is assumed to be homogeneous, anisotropic and linear with the generalized moduli E_{iJKm} fully prescribed. The crack surface is described mathematically by two coincident surfaces, represented by the lower crack surface S_c^- and the upper crack surface S_c^+. The outward unit normal vectors of the two surfaces are denoted by $\boldsymbol{n}^-$ and $\boldsymbol{n}^+$, respectively. The medium is loaded by a uniform remote electrical/mechanical field but the body electrical charge and the body force are negligible. Also, it is assumed that the crack surface is smooth (i.e., the outward unit normal vector is uniquely defined) and the condition on the crack surface (i.e., termed the crack-face condition) is governed by one of the four crack-face conditions indicated further below. It is significant to note that while only a single crack is illustrated in Figure 2.1, the development of both the formulation and solution technique is also applicable to multiple cracks by simply considering S_c^- and S_c^+ as the combination of all lower crack surfaces and upper crack surfaces, respectively.

Besides basic field equations described above, the crack-face condition is found essential in the modeling of cracks in linear piezoelectric materials. Such crack-face boundary condition must be properly prescribed a priori in the analysis and it exhibits a significant influence on the near-front responses and fracture information on the crack boundary. In the present investigation, following four mathematical models used to simulate the condition on the crack surface are considered: electrically permeable, electrically impermeable, electrically semi-permeable, and energetically consistent crack-face models. These four different crack-face models can be separated into two categories, one containing the first two models where the prescribed mechanical and electrical conditions are fully uncoupled whereas the other containing the last two models with fully coupled mechanical/electrical conditions being prescribed (see details in Rungamornrat et al (2015)).

For an impermeable crack-face condition, the jump in the crack-face generalized displacement, defined by $\Delta u_J \equiv u_J^+ - u_J^-$, is unknown a priori whereas the crack-face generalized tractions, defined by t_I^+ and t_I^-, are completely known. For a permeable crack-face condition, the jump in the crack-face displacement Δu_i and the

crack-face surface electrical charge t_4^+ are unknown whereas the mechanical tractions t_i^+ and t_i^- are known and the jump in the crack-face electrical potential Δu_4 and the sum of the crack-face surface electrical charges (i.e., $\Sigma t_4 \equiv t_4^+ + t_4^-$) vanish. For an electrically semi-permeable crack-face condition, the crack-face tractions t_i^+ and t_i^- are completely known whereas the sum of the crack-face surface electrical charge Σt_4 vanishes. In addition, the jump in the crack-face generalized displacement Δu_J and the crack-face surface electrical charge t_4^+ are fully unknown and they satisfy the following relation (see Rungamornrat et al. (2015))

$$t_4^+ \Delta u_i n_i^+ = -\kappa_c \Delta u_4 \tag{2.6}$$

where the constant κ_c denotes the dielectric permittivity of ta medium filled within the crack cavity. To easily provide the description of the last crack-face condition, the mechanical tractions on the lower crack surface and upper crack surface t_i^+ and t_i^- can be separated into two parts such that $t_i^+ = \sigma_i^+ + \tau_i^+$ and $t_i^- = \sigma_i^- + \tau_i^-$ where $\left\{\sigma_i^+, \sigma_i^-\right\}$ and $\left\{\tau_i^+, \tau_i^-\right\}$ represent the normal and shear tractions, respectively. For an energetically consistent crack-face model, the shear traction on both crack surfaces $\left\{\tau_i^+, \tau_i^-\right\}$ are completely known whereas the sum of the crack-face surface electrical charge Σt_4 and the sum of the crack-face normal tractions (i.e., $\Sigma \sigma_i \equiv \sigma_i^+ + \sigma_i^-$) vanish. In addition, the jump in the crack-face generalized displacement Δu_J, the crack-face normal traction σ_i^+, and the crack-face surface electrical charge t_4^+ are fully unknown and they must satisfy (2.6) and the following condition

$$2\sigma = \kappa_c \left(\Delta u_4\right)^2 / \left(\Delta u_i n_i^+\right)^2 \tag{2.7}$$

where $\sigma = \sigma_i^+ n_i^+$ denotes the normal mechanical traction. It is emphasized that the superscripts " – " and " + " are employed to designate quantities associated with the lower crack surface and upper crack surface, respectively.

2.3 STANDARD INTEGRAL RELATION

A boundary element method is based primarily on a system of boundary integral equations established from the basic field equations (2.4) and (2.5) in another form containing merely quantities on the domain boundary and crack surface. In the absence of the body electrical charge, the body force, and remote mechanical and electrical loadings, the generalized stress σ_{IK} and the generalized displacement u_P at any point $\boldsymbol{x}$ in a piezoelectric whole space containing cracks can be established in terms of data on the crack surface $\Sigma t_J = t_J^+ + t_J^-$ and $\Delta u_J = u_J^+ - u_J^-$ as

$$u_P(\boldsymbol{x}) = \int_{S^+} U_J^P(\boldsymbol{\xi}-\boldsymbol{x})\Sigma t_J(\boldsymbol{\xi})dA(\boldsymbol{\xi}) - \int_{S^+} S_{iJ}^P(\boldsymbol{\xi}-\boldsymbol{x})n_i(\boldsymbol{\xi})\Delta u_J(\boldsymbol{\xi})dA(\boldsymbol{\xi}) \tag{2.8}$$

$$\sigma_{lK}(\boldsymbol{x}) = -\int_{S^+} S_{lJ}^K(\boldsymbol{\xi}-\boldsymbol{x})\Sigma t_J(\boldsymbol{\xi})dA(\boldsymbol{\xi}) + \int_{S^+} \Sigma_{iJ}^{lK}(\boldsymbol{\xi}-\boldsymbol{x})n_i(\boldsymbol{\xi})\Delta u_J(\boldsymbol{\xi})dA(\boldsymbol{\xi}) \tag{2.9}$$

where $U_J^P(\boldsymbol{\xi}-\boldsymbol{x})$, $S_{iJ}^P(\boldsymbol{\xi}-\boldsymbol{x})$, and $\Sigma_{iJ}^{lK}(\boldsymbol{\xi}-\boldsymbol{x})$ are known functions associated with a piezoelectric state of an infinite medium under a unit concentrated body force and electric charge. The explicit expressions of these Green' functions for an anisotropic, linear piezoelectric solid are given by (see Rungamornrat and Mear (2008a))

$$U_J^P(\boldsymbol{\xi}-\boldsymbol{x}) = \frac{1}{8\pi^2 r}\oint_{\boldsymbol{z}\cdot\boldsymbol{r}=0} (\boldsymbol{z},\boldsymbol{z})_{JP}^{-1} ds(\boldsymbol{z}) \tag{2.10}$$

$$S_{iJ}^P(\boldsymbol{\xi}-\boldsymbol{x}) = E_{iJKl}\frac{\partial U_K^P(\boldsymbol{\xi}-\boldsymbol{x})}{\partial \xi_l} \tag{2.11}$$

$$\Sigma_{iJ}^{lK}(\boldsymbol{\xi}-\boldsymbol{x}) = E_{lKPq}\frac{\partial S_{iJ}^P(\boldsymbol{\xi}-\boldsymbol{x})}{\partial \xi_q} \tag{2.12}$$

where $\boldsymbol{r} = \boldsymbol{\xi}-\boldsymbol{x}$; $r = \|\boldsymbol{r}\|$; $\boldsymbol{z}$ is a unit vector contained in a plane normal to the position vector $\boldsymbol{r}$; $(\boldsymbol{z},\boldsymbol{z})_{JP} = z_i E_{iJPl} z_l$, $(\boldsymbol{z},\boldsymbol{z})^{-1}$ represents an inverse of the matrix $(\boldsymbol{z},\boldsymbol{z})$; and the line integral in (2.10) must be carried out over a unit circle $\|\boldsymbol{z}\| = 1$ on the plane $\boldsymbol{z}\cdot\boldsymbol{r} = 0$. It is important to remark that all two-point functions $U_J^P(\boldsymbol{\xi}-\boldsymbol{x})$, $S_{iJ}^P(\boldsymbol{\xi}-\boldsymbol{x})$, and $\Sigma_{iJ}^{lK}(\boldsymbol{\xi}-\boldsymbol{x})$ are singular at $\boldsymbol{\xi} = \boldsymbol{x}$ of order $\mathcal{O}(1/r)$, $\mathcal{O}(1/r^2)$, and $\mathcal{O}(1/r^3)$, respectively. It is remarked that the boundary integral relations (2.8) and (2.9) render

the generalized displacement and the generalized stress at any point within the body to be calculated once the unknown jump in the crack-face generalized displacement is solved. By forming a proper limiting process $\boldsymbol{x} \to \boldsymbol{y} \in S_c^+$ of the relation (2.8), it leads to an integral equation for the sum of the crack-face generalized displacement $\Sigma \boldsymbol{u}_P$:

$$\frac{1}{2}\Sigma u_P(\boldsymbol{y}) = \int_{S^+} U_J^P(\boldsymbol{\xi}-\boldsymbol{x})\Sigma t_J(\boldsymbol{\xi})\,dA(\boldsymbol{\xi}) - \int_{S^+} S_{iJ}^P(\boldsymbol{\xi}-\boldsymbol{x}) n_i(\boldsymbol{\xi})\Delta u_J(\boldsymbol{\xi})\,dA(\boldsymbol{\xi}) \qquad (2.13)$$

The boundary integral equation (2.13) possesses following key features: (i) it involves only the known sum of the crack-face generalized traction $\Sigma \boldsymbol{t}_P$; (ii) it contains two unknown crack-face data $\Sigma \boldsymbol{u}_P$ and $\Delta \boldsymbol{u}_P$; and (iii) the first integral involves the weakly singular kernel $U_J^P(\boldsymbol{\xi}-\boldsymbol{x})$ which can be evaluated using the concept of Riemann whereas the second integral involves the strongly singular kernel $S_{iJ}^P(\boldsymbol{\xi}-\boldsymbol{x})$ which must be interpreted in the sense of Cauchy. It is crucial to point out that only the integral relation (2.13) is not adequate for solving both the unknowns $\Sigma \boldsymbol{u}_P$ and $\Delta \boldsymbol{u}_P$ on the crack surface. This stems directly from that the boundary integral equation (2.13) is mathematically degenerate and cannot differentiate two problems involving the same crack subjected to different self-equilibrated, crack-face generalized traction (i.e., $\Sigma \boldsymbol{t}_P = \boldsymbol{0}$ for both cases).

By multiplying equation (2.9) by an outward unit normal vector $\boldsymbol{n}^+$ at any point $\boldsymbol{y} \in S_c^+$ and taking a proper limiting process $\boldsymbol{x} \to \boldsymbol{y} \in S_c^+$, it yields the boundary integral equation for the jump in the crack-face generalized traction $\Delta \boldsymbol{t}_K = \boldsymbol{t}_K^+ - \boldsymbol{t}_K^-$:

$$\begin{aligned}\frac{1}{2}\Delta t_K(\boldsymbol{y}) = &-\int_{S^+} S_{lJ}^K(\boldsymbol{\xi}-\boldsymbol{x}) n_l(\boldsymbol{y})\Sigma t_J(\boldsymbol{\xi})\,dA(\boldsymbol{\xi}) \\ &+ \int_{S^+} \Sigma_{iJ}^{lK}(\boldsymbol{\xi}-\boldsymbol{x}) n_l(\boldsymbol{\xi}) n_i(\boldsymbol{\xi})\Delta u_J(\boldsymbol{\xi})\,dA(\boldsymbol{\xi})\end{aligned} \qquad (2.14)$$

The boundary integral equation (2.14) possesses following important features: (i) it contain the complete information of the crack-face generalized tractions $\Delta \boldsymbol{t}_K$ and $\Sigma \boldsymbol{t}_J$; (ii) it contains only one unknown function $\Delta \boldsymbol{u}_J$; and (iii) the first integral involves the strongly singular kernel $S_{lJ}^K(\boldsymbol{\xi}-\boldsymbol{x})$ which must be interpreted in the sense of Cauchy

whereas the second integral involves the hyper-singular kernel $\Sigma_{iJ}^{lK}\left(\boldsymbol{\xi}-\boldsymbol{x}\right)$ which must be interpreted using the concept of Hadamard finite part integrals. The features (i) and (ii) render the integral equation (2.14) sufficient for solving the unknown relative crack-face generalized displacement $\Delta\boldsymbol{u}_J$. Once $\Delta\boldsymbol{u}_J$ is determined, the sum of the crack-face, generalized displacement $\Sigma\boldsymbol{u}_P$ can be obtained from the integral equation (2.13).

While the standard boundary integral equations (2.13) and (2.14) provide a sufficient basis for the modeling of fractures in a linear piezoelectric medium, use of those equations still requires the nontrivial treatment of both hyper-singular and strongly singular integrals in the numerical implementations.

2.4 REGULARIZED INTEGRAL RELATIONS/EQUATIONS

To circumvent the treatment of hypersingular and strongly singular integrals, completely regularized boundary integral equations are established utilizing the same procedure suggested by Rungamornrat and Mear (2008a, 2008b) and Pongtinnaboot et al. (2011). In their study, a systematic regularization procedure is utilized to treat cracks in both infinite and finite domains. The important component used in such regularization procedure is the interchange of derivatives between the kernels and the boundary data via the integration-by-parts technique with Stokes' theorem. From this regularization procedure, the strongly singular kernel $S_{iJ}^{P}\left(\boldsymbol{\xi}-\boldsymbol{x}\right)$ and the hypersingular kernel $\Sigma_{iJ}^{lK}\left(\boldsymbol{\xi}-\boldsymbol{x}\right)$ are represented in following form

$$S_{iJ}^{P}\left(\boldsymbol{\xi}-\boldsymbol{x}\right)=H_{iJ}^{P}\left(\boldsymbol{\xi}-\boldsymbol{x}\right)+\varepsilon_{ism}\frac{\partial G_{mJ}^{P}\left(\boldsymbol{\xi}-\boldsymbol{x}\right)}{\partial\xi_s} \tag{2.15}$$

$$\Sigma_{iJ}^{lK}\left(\boldsymbol{\xi}-\boldsymbol{x}\right)=-E_{iJKl}\left(\boldsymbol{\xi}-\boldsymbol{x}\right)+\varepsilon_{ism}\frac{\partial}{\partial\xi_s}\varepsilon_{lrt}\frac{\partial}{\partial\xi_r}C_{mJ}^{tK}\left(\boldsymbol{\xi}-\boldsymbol{x}\right) \tag{2.16}$$

where ε_{ism} denotes an alternating tensor, $\delta\left(\boldsymbol{\xi}-\boldsymbol{x}\right)$ denotes a Dirac-delta distribution with the center at a point $\boldsymbol{x}$, and the functions $H_{iJ}^{P}\left(\boldsymbol{\xi}-\boldsymbol{x}\right)$, $G_{mJ}^{P}\left(\boldsymbol{\xi}-\boldsymbol{x}\right)$, and $C_{mJ}^{tK}\left(\boldsymbol{\xi}-\boldsymbol{x}\right)$ are defined by (see Rungamornrat and Mear (2008b) and Rungamornrat and Senjuntichai (2009))

$$H_{iJ}^{P}\left(\boldsymbol{\xi}-\boldsymbol{x}\right)=-\frac{1}{4\pi r^{3}}\delta_{JP}\left(\xi_{i}-x_{i}\right) \tag{2.17}$$

$$G_{mJ}^{P}\left(\boldsymbol{\xi}-\boldsymbol{x}\right)=\frac{\varepsilon_{mqa}E_{qJKl}}{8\pi^{2}r}\oint_{\mathbf{z}\cdot\boldsymbol{r}=0}\left(\mathbf{z},\mathbf{z}\right)_{KP}^{-1}z_{a}z_{l}ds\left(\mathbf{z}\right) \tag{2.18}$$

$$C_{mJ}^{tK}\left(\boldsymbol{\xi}-\boldsymbol{x}\right)=\frac{A_{mtsl}^{KJPQ}}{8\pi^{2}r}\oint_{\mathbf{z}\cdot\boldsymbol{r}=0}\left(\mathbf{z},\mathbf{z}\right)_{PQ}^{-1}z_{s}z_{l}ds\left(\mathbf{z}\right) \tag{2.19}$$

with δ_{JP} denotes the generalized Kronecker delta and a material-dependent constant A_{mtsl}^{KJPQ} defined by

$$A_{mtsl}^{KJPQ}=\varepsilon_{aum}\varepsilon_{adt}\left\{E_{uKPs}E_{dJQl}-\frac{1}{4}E_{dJKu}E_{lPQs}\right\} \tag{2.20}$$

It is apparent that the function $H_{iJ}^{P}\left(\boldsymbol{\xi}-\boldsymbol{x}\right)$ is free of material constants and singular at a point $\boldsymbol{\xi}=\boldsymbol{x}$ of $\mathcal{O}\left(1/r^{2}\right)$ while the functions $G_{mJ}^{P}\left(\boldsymbol{\xi}-\boldsymbol{x}\right)$ and $C_{mJ}^{tK}\left(\boldsymbol{\xi}-\boldsymbol{x}\right)$ are clearly singular only at a point $\boldsymbol{\xi}=\boldsymbol{x}$ of $\mathcal{O}\left(1/r\right)$.

By applying the two representations (2.15) and (2.16) to the standard integral relations (2.8) and (2.9) and then integrating terms involving the functions $G_{mJ}^{P}\left(\boldsymbol{\xi}-\boldsymbol{x}\right)$ and $C_{mJ}^{tK}\left(\boldsymbol{\xi}-\boldsymbol{x}\right)$ by parts via Stokes' theorem, the regularized integral relations for both the generalized stress and the generalized displacement are expressed as

$$\begin{aligned}u_{P}\left(\boldsymbol{x}\right)=&\int_{S_{c}^{+}}U_{J}^{P}\left(\boldsymbol{\xi}-\boldsymbol{x}\right)\Sigma t_{J}\left(\boldsymbol{\xi}\right)dA\left(\boldsymbol{\xi}\right)-\int_{S_{c}^{+}}H_{iJ}^{P}\left(\boldsymbol{\xi}-\boldsymbol{x}\right)n_{i}\left(\boldsymbol{\xi}\right)\Delta u_{J}\left(\boldsymbol{\xi}\right)dA\left(\boldsymbol{\xi}\right)\\&+\int_{S_{c}^{+}}G_{mJ}^{P}\left(\boldsymbol{\xi}-\boldsymbol{x}\right)D_{m}\Delta u_{J}\left(\boldsymbol{\xi}\right)dA\left(\boldsymbol{\xi}\right)\end{aligned} \tag{2.21}$$

$$\begin{aligned}\sigma_{lK}\left(\boldsymbol{x}\right)=&\varepsilon_{lrt}\frac{\partial}{\partial x_{r}}\left\{\int_{S_{c}^{+}}G_{tK}^{P}\left(\boldsymbol{\xi}-\boldsymbol{x}\right)\Sigma t_{J}\left(\boldsymbol{\xi}\right)dA\left(\boldsymbol{\xi}\right)+\int_{S_{c}^{+}}C_{mJ}^{tK}\left(\boldsymbol{\xi}-\boldsymbol{x}\right)D_{m}\left(\boldsymbol{\xi}\right)\Delta u_{J}\left(\boldsymbol{\xi}\right)dA\left(\boldsymbol{\xi}\right)\right\}\\&-\int_{S_{c}^{+}}H_{lK}^{J}\left(\boldsymbol{\xi}-\boldsymbol{x}\right)\Sigma t_{J}\left(\boldsymbol{\xi}\right)dA\left(\boldsymbol{\xi}\right)\end{aligned} \tag{2.22}$$

where $D_{m}\left(\cdot\right)=n_{i}\varepsilon_{ism}\partial\left(\cdot\right)/\partial\xi_{s}$ denotes the surface differential operator. This set of regularized integral relations can be employed as an alternative to the standard integral relations (2.8) and (2.9) in the post-process of the generalized stresses and the

generalized displacements at any point within the medium after the relative crack-face generalized displacement $\Delta \boldsymbol{u}_J$ is solved.

By taking the limit $\boldsymbol{x} \to \boldsymbol{y} \in S_c^+$ of the integral relation (2.21), it results in an alternative integral equation for the sum of the crack-face generalized displacement. By further multiplying this equation by a well-behaved test function $\tilde{t}_P$ and then performing the integration over the entire crack surface, it leads to the weakly singular weak-form boundary integral equation for the sum of the crack-face generalized displacement:

$$\begin{aligned}\frac{1}{2}\int_{S_c^+} \tilde{t}_P(\boldsymbol{y})\Sigma u_P(\boldsymbol{y})\,dA(\boldsymbol{y}) = &\int_{S_c^+} t_P(\boldsymbol{y}) \int_{S_c^+} U_J^P(\boldsymbol{\xi}-\boldsymbol{x})\Sigma t_J(\boldsymbol{\xi})\,dA(\boldsymbol{\xi})dA(\boldsymbol{y}) \\ &- \int_{S_c^+} t_P(\boldsymbol{y}) \int_{S_c^+} H_{iJ}^P(\boldsymbol{\xi}-\boldsymbol{x}) n_i(\boldsymbol{\xi})\Delta u_J(\boldsymbol{\xi})\,dA(\boldsymbol{\xi})dA(\boldsymbol{y}) \\ &+ \int_{S_c^+} t_P(\boldsymbol{y}) \int_{S_c^+} G_{mJ}^P(\boldsymbol{\xi}-\boldsymbol{x}) D_m \Delta u_J(\boldsymbol{\xi})\,dA(\boldsymbol{\xi})dA(\boldsymbol{y})\end{aligned} \tag{2.23}$$

Similarly, the alternative form of the integral equation for the jump in the crack-face generalized traction (2.14) can be alternatively established by taking the product $\sigma_{lK}(\boldsymbol{x}) n_l^+(\boldsymbol{y})$ of the integral relation (2.22) and then carrying out the limit $\boldsymbol{x} \to \boldsymbol{y} \in S_c^+$. By multiplying the generalized traction integral equation by an arbitrary well-behaved test function $\tilde{u}_K$, then performing the integration over the entire crack surface, and finally utilizing Stokes' theorem to carry out the integration by parts of an integral associated with the function $C_{mJ}^{tK}(\boldsymbol{\xi}-\boldsymbol{x})$, it gives rise to

$$\begin{aligned}\frac{1}{2}\int_{S_c^+} \tilde{u}_K(\boldsymbol{y})\Delta t_K(\boldsymbol{y})\,dA(\boldsymbol{y}) = &-\int_{S_c^+} D_t \tilde{v}_K(\boldsymbol{y}) \int_{S_c^+} C_{mJ}^{tK}(\boldsymbol{\xi}-\boldsymbol{x}) D_m \Delta u_J(\boldsymbol{\xi})\,dA(\boldsymbol{\xi})dA(\boldsymbol{y}) \\ &- \int_{S_c^+} D_t \tilde{v}_K(\boldsymbol{y}) \int_{S_c^+} G_{tK}^J(\boldsymbol{\xi}-\boldsymbol{x})\Sigma t_J(\boldsymbol{\xi})\,dA(\boldsymbol{\xi})dA(\boldsymbol{y}) \\ &+ \int_{S_c^+} \tilde{v}_K(\boldsymbol{y}) \int_{S_c^+} H_{iK}^J(\boldsymbol{\xi}-\boldsymbol{x}) n_i(\boldsymbol{y})\Sigma t_J(\boldsymbol{\xi})\,dA(\boldsymbol{\xi})dA(\boldsymbol{y})\end{aligned} \tag{2.24}$$

It is vital to point out that the weak-form boundary integral equations (2.23) and (2.24) are fully regularized in that the kernels $U_J^P(\boldsymbol{\xi}-\boldsymbol{x})$, $H_{iJ}^P(\boldsymbol{\xi}-\boldsymbol{x})n_i(\boldsymbol{\xi})$,

$H_{iK}^{J}(\boldsymbol{\xi}-\boldsymbol{x})n_i(\boldsymbol{y})$, $G_{mJ}^{P}(\boldsymbol{\xi}-\boldsymbol{x})$, $C_{mJ}^{tK}(\boldsymbol{\xi}-\boldsymbol{x})$ are weakly singular of $\mathcal{O}(1/r)$. This pair of weakly singular, weak-form, boundary integral equations provides a complete basis for determining crack-face unknown data.

CHAPTER 3
SOLUTION PROCEDURE

This chapter presents briefly the solution methodology for determining the jump in and sum of the crack-face generalized displacement, keys ingredient of a computational procedure based upon the weakly singular boundary-based method and standard Galerkin technique, and the post-process for the generalized T-stress from the solved data on the crack surface.

3.1 SOLUTION METHODOLOGY

The weakly singular, weak-form integral equations for the sum of the crack-face generalized displacement (2.23) and the jump in the crack-face generalized traction (2.24) provide a complete set of governing integral equations for determining the unknown crack-face data Δu_P and Σu_P. Both the integral equations (2.23) and (2.24) can be re-expressed in a form convenient for further reference as

$$\mathcal{D}(\tilde{t},\Sigma u)=\mathcal{U}(\tilde{t},\Sigma t)+\mathcal{G}(\tilde{t},\Delta u)+\mathcal{H}(\tilde{t},\Delta u) \tag{3.1}$$

$$\mathcal{C}(\tilde{u},\Delta u)=\mathcal{G}(\Sigma t,\tilde{u})+\mathcal{H}(\Sigma t,\tilde{u})+\mathcal{D}(\tilde{u},\Delta t) \tag{3.2}$$

where all bilinear and linear integral operators are given explicitly by

$$\mathcal{U}(X,Y)=\int_{S_c^+} X_P(y)\int_{S_c^+} U_J^P(\xi-x)Y_J(\xi)\,dA(\xi)dA(y) \tag{3.3}$$

$$\mathcal{C}(X,Y)=-\int_{S_c^+} D_t X_K(y)\int_{S_c^+} C_{mJ}^{tK}(\xi-x)D_m Y_J(\xi)\,dA(\xi)dA(y) \tag{3.4}$$

$$\mathcal{G}(X,Y)=\int_{S_c^+} X_P(y)\int_{S_c^+} G_{mJ}^{P}(\xi-x)D_m Y_J(\xi)\,dA(\xi)dA(y) \tag{3.5}$$

$$\mathcal{H}(X,Y)=-\int_{S_c^+} X_P(y)\int_{S_c^+} H_{iJ}^{P}(\xi-x)n_i(\xi)Y_J(\xi)\,dA(\xi)dA(y) \tag{3.6}$$

$$\mathcal{D}(X,Y)=-\frac{1}{2}\int_{S_c^+} X_K(y)Y_K(y)\,dA(y) \tag{3.7}$$

where $\boldsymbol{X}$ and $\boldsymbol{Y}$ are any four-component vectors. It is crucial to remark that the linear integral operators $\boldsymbol{\mathcal{C}}$ and $\boldsymbol{\mathcal{D}}$ given by (3.4) and (3.7) are in a symmetric form (i.e., $\boldsymbol{\mathcal{C}}(\boldsymbol{X},\boldsymbol{Y})=\boldsymbol{\mathcal{C}}(\boldsymbol{Y},\boldsymbol{X})$ and $\boldsymbol{\mathcal{D}}(\boldsymbol{X},\boldsymbol{Y})=\boldsymbol{\mathcal{D}}(\boldsymbol{Y},\boldsymbol{X})$. It is also evident from the system of boundary integral equations (3.1) and (3.2) that they are fully coupled through the jump in the crack-face generalized displacement Δu_p and the weakly singular, weak-form boundary integral equation for the jump in the crack-face generalized traction does not contain the sum of the crack-face generalized displacement Σu_p. As a result, Δu_p is obtained first by solving the integral equation (3.2) along with the prescribed crack-face condition using weakly singular SGBEM and Galerkin technique similar to the work of Rungamornrat et al. (2015). It should be remarked that for the case of energetically consistent and electrically semi-permeable cracks, additional crack-face conditions (2.6) and (2.7) must be properly integrated in the solution procedure and the resulting set of nonlinear equations must be solved via a selected efficient nonlinear solver. After Δu_p is determined, the weak-form integral equation (3.1) can be subsequently solved by the standard Galerkin scheme to obtain the sum of the crack-face generalized displacement Σu_p. Once all the unknown crack-face data is known, the generalized T-stress can be obtained by post-processing the solution of Σu_p in the neighborhood of the crack front.

3.2 SOLUTION DISCRETIZATION

By introducing Galerkin approximation to a set of weakly singular integral equations (3.1) and (3.2), it leads to two sets of linear equations:

$$[\mathbf{D}][\Sigma\mathbf{U}]=[\mathbf{U}\quad \mathbf{G}+\mathbf{H}]\begin{bmatrix}\Sigma\mathbf{T}\\ \Delta\mathbf{U}\end{bmatrix} \tag{3.8}$$

$$[\mathbf{C}][\Delta\mathbf{U}]=[\mathbf{G}+\mathbf{H}\quad \hat{\mathbf{D}}]\begin{bmatrix}\Sigma\mathbf{T}\\ \Delta\mathbf{T}\end{bmatrix} \tag{3.9}$$

where sub-matrices $\mathbf{C},\{\mathbf{D},\hat{\mathbf{D}}\},\mathbf{G},\mathbf{H},\mathbf{U}$ are associated with the linear integral operators $\boldsymbol{\mathcal{C}},\boldsymbol{\mathcal{D}},\boldsymbol{\mathcal{G}},\boldsymbol{\mathcal{H}},\boldsymbol{\mathcal{U}}$ respectively; $\Sigma\mathbf{U}$ and $\Delta\mathbf{U}$ are nodal vectors associated with the sum of and the jump in the crack-face generalized displacements, respectively; and $\Sigma\mathbf{T}$

and $\Delta\mathbf{T}$ are vectors of nodal quantities associated with the sum of and the jump in the crack-face generalized tractions, respectively. To enhance the approximation of the relative crack-face displacement, special elements developed by Rungamornrat and Mear (2008a) are utilized to discretize the near-front field. Shape functions of these special elements are enhanced to contain the right near-front square-root behavior and they, as a result, can capture the near-front singularity accurately by using relatively large element size.

To treat energetically consistent and electrically semi-permeable cracks, additional crack-face conditions (2.6) and (2.7) are enforced weakly using a standard weighted residual procedure. The resulting weak-forms of both (2.6) and (2.7) is given by (see also the work of Rungamornrat et al. (2015))

$$\int_{S_c^+} \hat{w}(\boldsymbol{y})\left\{\kappa_c \Delta u_4(\boldsymbol{y}) + t_4^+(\boldsymbol{y})\Delta u_j(\boldsymbol{y}) n_j^+(\boldsymbol{y})\right\} dA(\boldsymbol{y}) = 0 \tag{3.10}$$

$$\int_{S_c^+} \hat{w}(\boldsymbol{y})\left\{2\kappa_c \sigma(\boldsymbol{y}) - \left[t_4^+(\boldsymbol{y})\right]^2\right\} dA(\boldsymbol{y}) = 0 \tag{3.11}$$

where $\hat{w}$ is a square-integrable test function. By following Galerkin technique along with the discretization of the t_4^+, Δu_i and Δu_4 described above, the approximate version of (3.10) and (3.11) can be expressed as

$$\mathbf{f}\left(\Delta\mathbf{U}^e, \Delta\mathbf{U}^m, \mathbf{T}^{e+}\right) = 0 \tag{3.12}$$

$$\mathbf{g}\left(\mathbf{T}^{mn}, \mathbf{T}^{e+}\right) = 0 \tag{3.13}$$

where $\Delta\mathbf{U}^e$ denotes a nodal vector corresponding to the discretization of Δu_4; $\Delta\mathbf{U}^m$ denotes a nodal vector corresponding to the discretization of Δu_i; $\mathbf{T}^{e+}$ denotes a nodal vector corresponding to the discretization of t_4^+; $\mathbf{T}^{mn}$ denotes a nodal vector corresponding to the discretization of the mechanical normal traction σ; and $\mathbf{f}$ and $\mathbf{g}$ are systems of nonlinear algebraic equations with their function form defined by the weak-forms (3.10) and (3.11), respectively.

3.3 NUMERICAL INTEGRATION

While the sub-matrices $\mathbf{D}$ and $\hat{\mathbf{D}}$ obtained from the approximation of a single surface integral can be readily evaluated using Gaussian quadrature, the computation of the sub-matrices $\mathbf{C},\mathbf{G},\mathbf{H}$ and $\mathbf{U}$ needs more extensive calculations of double surface integrals containing weakly singular kernels $C_{mJ}^{tK},G_{mJ}^{P},H_{iJ}^{P}n_i,U_J^P$ for a pair of elements from the approximation of the crack surface. All involved double surface integrals over a pair of elements can be separated into three groups depending on the characteristic of the integrand. The first group contains double surface integrals associated with pairs of remote finite elements. Due to the well-behaved integrand, integrals in this group can be efficiently and accurately integrated by Gaussian quadrature. The second group contains double surface integrals over a pair of identical finite elements. For this particular case, it is apparent that the involved integrands are weakly singular. Although the integrals exist in the sense of Riemann, the direct integration of these integrals using Gaussian quadrature is computationally inefficient as pointed out by Xiao (1998). To circumvent this problem, a systematic technique via a triangular polar transformation and other related changes of variables suggested by Xiao (1998) is exploited to regularize the weakly singular integrand. The singularity-free double surface integrals are then integrated by Gaussian quadrature. The final group contains double surface integrals over pairs of adjacent or relatively close finite elements. In this case, the involved integrand is nearly singular and possesses the rapid variation characteristic. Again, it was pointed out by Xiao (1998) that this particular type of integrals is difficult to be treated and the standard Gaussian quadrature alone cannot be used to efficiently integrate such nearly singular integrals. In the present study, the systematic technique suggested by Xiao (1998) is adopted. In particular, a family of variable transformations is employed first to regularize the integrand behavior and then Gaussian quadrature is applied to integrate the resulting well-behaved integrals.

To build the system of nonlinear algebraic equations (3.12) and (3.13), all involved integrals contain only regular functions (e.g., shape functions and prescribed data) and they are given in a form of single surface integrals over elements obtained

from the approximation of the crack surface. Standard Gaussian quadrature can be subsequently applied to efficiently and accurately integral all those integrals.

3.4 EVALUATION OF INVOLVED KERNELS

To additionally lower the computational resource needed to construct all involved coefficient matrices in a set of linear equations (3.8)-(3.9), all involved kernels $H_{iJ}^{P}n_i, C_{mJ}^{tK}, G_{mJ}^{P}, U_J^P$ have to be calculated in an efficient fashion for every pair of field and source points $(\boldsymbol{\xi}, \boldsymbol{y})$. For the weakly singular kernel $H_{iJ}^{P}n_i$, it only requires the calculation of a unit vector n_i to the crack surface and the elementary function H_{iJ}^{P}, and this can be readily accomplished via a direct substitution and the geometric information of finite elements. For the last three weakly kernels, their expressions for generally anisotropic materials are derived in terms of a line integral over a unit circle. The direct computation of the contour integral for all pairs of source and field points $(\boldsymbol{\xi}, \boldsymbol{y})$ resulting from quadrature is clearly time demanding. To prevent such substantial calculation, an interpolation scheme (e.g., Rungamornrat and Mear (2008a, 2008b)) is employed to obtain the values of all involved kernels. In this technique, values of the kernels are first determined by directly integrating the line integrals (2.18) and (2.19) via Gaussian quadrature at all grid points and their interpolant is then established on a two-dimensional grid via standard local basis functions. The value of the kernels $C_{mJ}^{tK}, G_{mJ}^{P}, U_J^P$ at any pair of points $(\boldsymbol{\xi}, \boldsymbol{y})$ is then approximated by their interpolant and the accuracy can be enhanced by either increasing the degrees of basis functions or refining the grid size.

3.5 SOLVERS

To solve for the relative crack-face generalized displacement, a set of linear algebraic equations (3.9) must be solved together with the known crack-face boundary conditions. To aid following discussion, the vectors of nodal quantities $\Sigma\mathbf{T}$, $\Delta\mathbf{T}$ and $\Delta\mathbf{U}$ appearing in (3.9) can be partitioned into $\Sigma\mathbf{T} = \left[\Sigma\mathbf{T}^m \;\; \Sigma\mathbf{T}^e\right]$, $\Delta\mathbf{T} = \left[\Delta\mathbf{T}^m \;\; \Delta\mathbf{T}^e\right]$ and $\Delta\mathbf{U} = \left[\Delta\mathbf{U}^m \;\; \Delta\mathbf{U}^e\right]$ where the superscript "e" and "m" are employed to designate, respectively, the electrical and mechanical quantities. Furthermore, the

nodal quantities corresponding to the relative crack-face mechanical traction $\Delta\mathbf{T}^m$ can be decomposed into $\Delta\mathbf{T}^m = \Delta\mathbf{T}^{ms} + \Delta\mathbf{T}^{mn}$ where $\Delta\mathbf{T}^{ms}$ and $\Delta\mathbf{T}^{mn}$ denote the contribution from the shear and normal tractions, respectively.

For an impermeable crack-face model, the vectors $\Sigma\mathbf{T}$ and $\Delta\mathbf{T}$ are fully prescribed and, as a consequence, the set of linear equations (3.9) can be solved directly for the unknown $\Delta\mathbf{U}$ by a selected efficient linear solver such as a preconditioning conjugate gradient method. For a permeable crack, the mechanical traction data $\Sigma\mathbf{T}^m$ and $\Delta\mathbf{T}^m$ are completely known whereas the sum of the electrical tractions and the jump in the electric potential vanish (i.e., $\Sigma\mathbf{T}^e = \Delta\mathbf{U}^e = 0$). For this case, (3.9) is still adequate for determining the crack-face unknowns $\Delta\mathbf{U}^m$ and $\Delta\mathbf{T}^e$ and a partitioning scheme together with a preconditioning conjugate gradient method is adopted to determine the numerical solution.

For a semi-permeable crack-face model, the mechanical traction data $\Sigma\mathbf{T}^m$ and $\Delta\mathbf{T}^m$ are completely known; the sum of the electrical tractions disappears (i.e., $\Sigma\mathbf{T}^e = 0$); and the jump in the crack-face generalized displacement $\Delta\mathbf{U}$ and the jump in the crack-face electrical traction $\Delta\mathbf{T}^e = 2\mathbf{T}^{e+}$ are unknown a priori. To solve for these unknown crack-face data, (3.9) and a set of nonlinear algebraic equations (3.12) are solved simultaneously using Newton-Raphson iterative scheme. It should be remarked that each node on the crack surface contains five nodal unknowns, four associated with components of the relative crack-face generalized displacement and one corresponding to the jump in the electrical traction.

For an energetically consistent crack, the mechanical shear tractions $\Sigma\mathbf{T}^{ms}$ and $\Delta\mathbf{T}^{ms}$ are completely known; the sum of mechanical normal tractions and electrical tractions vanish (i.e., $\Sigma\mathbf{T}^e = \Sigma\mathbf{T}^{mn} = 0$); and the relative crack-face generalized displacement $\Delta\mathbf{U}$, the jump in the electrical traction $\Delta\mathbf{T}^e = 2\mathbf{T}^{e+}$, and the jump in the mechanical normal traction $\Delta\mathbf{T}^{mn} = 2\mathbf{T}^{mn}$ are unknown a priori. All these unknown crack-face data is solved from (3.9) and two systems of nonlinear algebraic equations (3.12)-(3.13) simultaneously using Newton-Raphson iterative scheme. For this particular case, each node on the crack surface involves six nodal unknowns, four associated with components of the relative crack-face generalized displacement, one

corresponding to the jump in the electrical traction and the other corresponding to the jump in the crack-face mechanical normal traction.

Once the relative crack-face generalized displacement $\Delta\mathbf{U}$ is solved for any type of crack-face conditions, this information serves as an input in the system of linear equations (3.8). The unknown sum of the nodal crack-face generalized displacements $\Sigma\mathbf{U}$ can then be obtained by solving (3.8) using a preconditioning conjugate gradient method.

3.6 CALCULATIONS OF GENERALIZED T-STRESS

Once the sum of the crack-face generalized displacement is completely determined, the generalized T-stress along the crack front can be extracted directly from this set of information as described, in detail, below.

Consider a crack-tip element with $\boldsymbol{x}_c$ denoting one of its nodes on the crack boundary. Let define $\{\boldsymbol{x}_c; x_1, x_2, x_3\}$ as a local reference Cartesian coordinate system with its origin located at $\boldsymbol{x}_c$ and $\{\boldsymbol{e}_1, \boldsymbol{e}_2, \boldsymbol{e}_3\}$ be a set of corresponding orthonormal base vectors as shown schematically in Figure 3.1. The generalized T-stress components referring to the defined local coordinate system are denoted by T_{11}, T_{13}, T_{33}, T_{14}, and T_{34} where the first three components are associated with the elastic T-stress and the last two correspond to the electrical T-stress. Values of the generalized T-stress components T_{11}, T_{13}, T_{33}, T_{14} and T_{34} at the nodal point $\boldsymbol{x}_c$ can be directly related to the finite part of the generalized strain tensor (combining the mechanical strain and the gradient of the electric potential) at a limiting point of $\boldsymbol{x}_c$ on the surface of the crack, denoted by ε_{iK}, via the following constitutive relation

$$T_{iJ} = E_{iJKl}\varepsilon_{lK} \tag{3.14}$$

where $T_{ij} = T_{ji}$, $\varepsilon_{ik} = \varepsilon_{ki}$, and the components T_{22}, T_{12}, T_{23}, and T_{24} are equal to the value of the generalized traction at a limiting point of $\boldsymbol{x}_c$ on the crack surface. For the impermeable case, T_{22}, T_{12}, T_{23}, and T_{24} are known a priori from the prescribed generalized traction; for the permeable case, T_{22}, T_{12}, T_{23} are known a priori from the

prescribed mechanical tractions and T_{24} is obtained from solving the system (3.15); for the semi-permeable case, T_{22}, T_{12}, T_{23} are known a priori from the prescribed mechanical tractions and T_{24} is obtained from solving the systems (3.15) and (3.18); and for the energetically consistent case, T_{12}, T_{23} are known a priori from the prescribed mechanical shear tractions and T_{22}, T_{24} are obtained from solving the systems (3.15), (3.18) and (3.19). The generalized strain components ε_{11}, ε_{13}, ε_{33}, ε_{14}, and ε_{34} can be computed from the information of the sum of the crack-face generalized displacement in the neighborhood of the point $\boldsymbol{x}_c$ via the following relations

$$\varepsilon_{11} = \frac{1}{2}\lim_{x\to x_c}\frac{\partial \Sigma u_1}{\partial x_1} = \frac{1}{2}\frac{\partial \Sigma u_1}{\partial x_1}(\boldsymbol{x}_c) \tag{3.15}$$

$$\varepsilon_{33} = \frac{1}{2}\lim_{x\to x_c}\frac{\partial \Sigma u_3}{\partial x_3} = \frac{1}{2}\frac{\partial \Sigma u_3}{\partial x_3}(\boldsymbol{x}_c) \tag{3.16}$$

$$\varepsilon_{13} = \frac{1}{4}\lim_{x\to x_c}\left\{\frac{\partial \Sigma u_1}{\partial x_3} + \frac{\partial \Sigma u_3}{\partial x_1}\right\} = \frac{1}{4}\left\{\frac{\partial \Sigma u_1}{\partial x_3} + \frac{\partial \Sigma u_3}{\partial x_1}\right\}(\boldsymbol{x}_c) \tag{3.17}$$

$$\varepsilon_{14} = \frac{1}{2}\lim_{x\to x_c}\frac{\partial \Sigma u_4}{\partial x_1} = \frac{1}{2}\frac{\partial \Sigma u_4}{\partial x_1}(\boldsymbol{x}_c) \tag{3.18}$$

$$\varepsilon_{34} = \frac{1}{2}\lim_{x\to x_c}\frac{\partial \Sigma u_4}{\partial x_3} = \frac{1}{2}\frac{\partial \Sigma u_4}{\partial x_3}(\boldsymbol{x}_c) \tag{3.19}$$

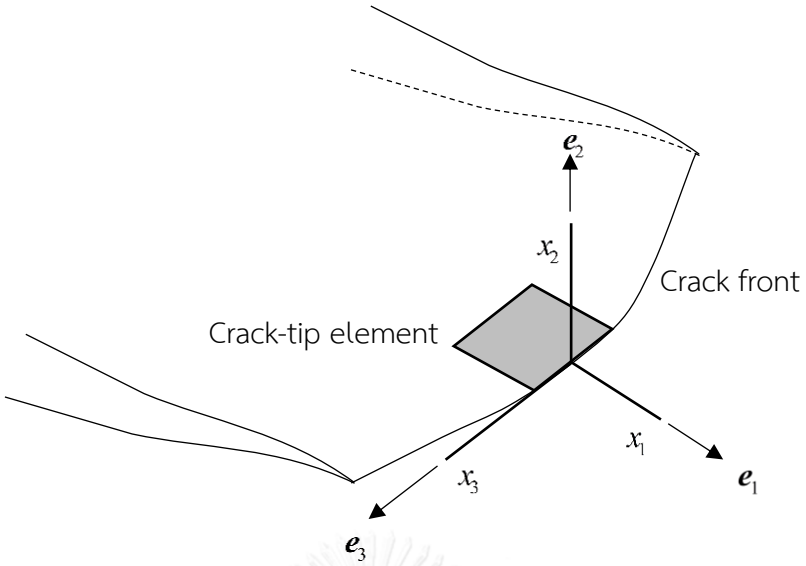

Figure 3.1 Schematic of crack-tip element and local reference coordinate system for calculation of generalized T-stress

The derivatives involved in the expressions (3.15)-(3.19) can be readily computed within the crack-tip elements. By using the known information of T_{22}, T_{12}, T_{23}, and T_{24} and the computed components ε_{11}, ε_{13}, ε_{33}, ε_{14}, and ε_{34}, the unknown generalized strain components ε_{22}, ε_{12}, ε_{23}, and ε_{24} and the generalized T-stress T_{11}, T_{13}, T_{33}, T_{14}, and T_{34} at the point $\boldsymbol{x}_c$ can be obtained by solving a set of nine linear equations (3.14).

CHAPTER 4
NUMERICAL RESULTS AND DISCUSSIONS

Computational efficiencies and accuracy of the proposed technique are fully explored by performing an extensive numerical experiment for various problems involving cracks in linear piezoelectric whole space under four different types of conditions on the crack surface including electrically permeable, electrically impermeable, electrically semi-permeable and energetically consistent conditions. A simple problem corresponding to a circular crack subjected to uniform remote and crack-face mechanical/electrical loadings is considered first and computed solutions are then benchmarked with existing analytical results to validate the integral formulation, the implemented solution procedure, and the post-process for the generalized T-stress. After the technique is fully tested, its vast capability is then demonstrated through the analysis of more complex problems involving nonaligned cracks, non-planar cracks and multiple cracks under general loading conditions.

To explore the convergence of computed solutions, a series of meshes with significantly different mesh sizes is adopted and used in the analysis. In the numerical study, the jump in the crack-face generalized displacement over the majority of the crack surface is discretized using standard, two-dimensional, six-node and eight-node isoparametric elements whereas that in a zone close to the crack boundary is discretized by nine-node special elements. The sum of the crack-face generalized displacement and other remaining crack-face unknowns over the entire crack surface are discretized by standard two-dimensional, isoparametric elements with the same mesh as that utilized for the discretization of the relative crack-face generalized displacement. A representative transversely isotropic, linear piezoelectric solid with elastic constants, dielectric permittivity and piezoelectric constants chosen to be the same as those of PZT-5H shown in Table 4.1 is employed for all cases considered in the numerical study presented further below.

Table 4.1 Elastic moduli, dielectric permittivities and piezoelectric constants of PZT-5H used in numerical study

Elastic constants (x 10^9 Pa)	E_{1111}	126.00
	E_{1122}	55.00
	E_{1133}	53.00
	E_{3333}	117.00
	E_{1313}	35.30
Piezoelectric constants (C/m^2)	E_{1143}	-6.50
	E_{3343}	23.30
	E_{1341}	17.00
Dielectric permittivities (x 10^{-9} C/(Vm))	$-E_{1441}$	15.10
	$-E_{3443}$	13.00

4.1 VERIFICATIONS

Consider a circular crack with the radius a contained in a linear piezoelectric whole space with the axis of material symmetry and poling direction coincident with the x_3 -axis as depicted in Figure 4.1(a). The crack front is described by

$$x_1 = a\cos\theta,\ x_2 = a\sin\theta,\ x_3 = 0 \tag{4.1}$$

where $\theta \in [0, 2\pi]$ denotes the angular position. The medium is subjected to four different loading conditions. The first two loading cases are associated with the uniform remote biaxial tension $\sigma_{33}^{\infty} = 2\sigma_{11}^{\infty} = 2\sigma_0$ (see Figure 4.1(b)) and the uniform remote electrical induction along the x_1- and x_3-axes $\sigma_{34}^{\infty} = 2\sigma_{14}^{\infty} = 2d_0$ (see Figure 4.1(c)) whereas the last two loading cases correspond to the uniformly distributed normal traction $t_3^+ = -t_3^- = \sigma_0$ (see Figure 4.2(a)) and the linearly distributed normal traction $t_3^+ = -t_3^- = \sigma_0\left(1 + x_1/a\right)/2$ (see Figure 4.2(b)). In the analysis, the values of σ_0 and d_0 are taken as $1\times10^6 \mathrm{N/m^2}$ and $1\times10^{-3}\mathrm{C/m^2}$, respectively, and three different meshes of

a crack indicated in Figure 4.3 are employed. The permittivity of a medium filled within the crack cavity is chosen to be $\kappa_c = 8.85\times10^{-12}\mathrm{C}/\left(\mathrm{Vm}\right)$ for both energetically consistent and electrically semi-permeable crack-face conditions. The normalized generalized T-stress components obtained from the proposed technique for all three meshes and four crack-face conditions are reported in Figure 4.4-4.8 along with the exact solutions established by Pich et al. (2015).

4.1.1 Uniform remote biaxial tension

For this particular loading case, only mechanical components of the generalized T-stress T_{11}, T_{33} and T_{13} are non-zero and a function of the angular position θ as shown in Figure 4.4-4.6. It is seen that the non-zero generalized T-stress components obtained from the three meshes for all four crack-face conditions show excellent agreement with the exact solutions. Specifically, the coarse mesh (i.e., Mesh-1) containing only eight elements can also yield sufficiently accurate results. Moreover, it can also reveal from results shown in Figures 4.4 and 4.5 that the generalized T-stresses components T_{11} and T_{33} are strongly dependent on the crack-face condition. On the contrary, the generalized T-stress component T_{13} is independent of the crack-face condition; computed values of T_{13} are identical for electrically permeable, electrically impermeable, electrically semi-permeable and energetically consistent cracks as clearly indicated in Figure 4.6.

4.1.2 Uniform remote electric induction in the both x_1–axis and x_3–axis

For this particular case, the generalized T-stress components T_{11} and T_{33} are identical and constant along the entire crack front but depend strongly on the crack-face condition as shown in Figure 4.7. In addition, it is found that the generalized T-stress components T_{11} and T_{33} vanishes for both permeable and semi-permeable cracks whereas those for the impermeable and energetically consistent cracks are of opposite sign.

In contrast with T_{11} and T_{33}, the generalized T-stress components T_{14} and T_{34} are dependent on the position on the crack boundary and the crack-face condition

play no role on the values of both T_{14} and T_{34} for this particular loading condition as shown in Figure 4.8. More specifically, the generalized T-stress components T_{14} and T_{34} are identical for all types of crack-face conditions treated.

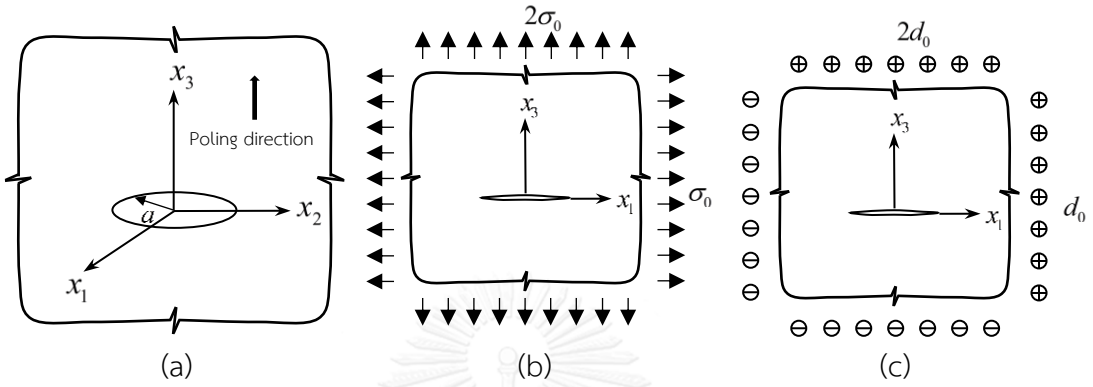

Figure 4.1 (a) Circular crack in piezoelectric whole space, (b) body under uniformly remote biaxial tension $\sigma_{33}^{\infty} = 2\sigma_{11}^{\infty} = 2\sigma_0$, and (c) body subjected to uniform remote electrical induction $\sigma_{34}^{\infty} = 2\sigma_{14}^{\infty} = 2d_0$

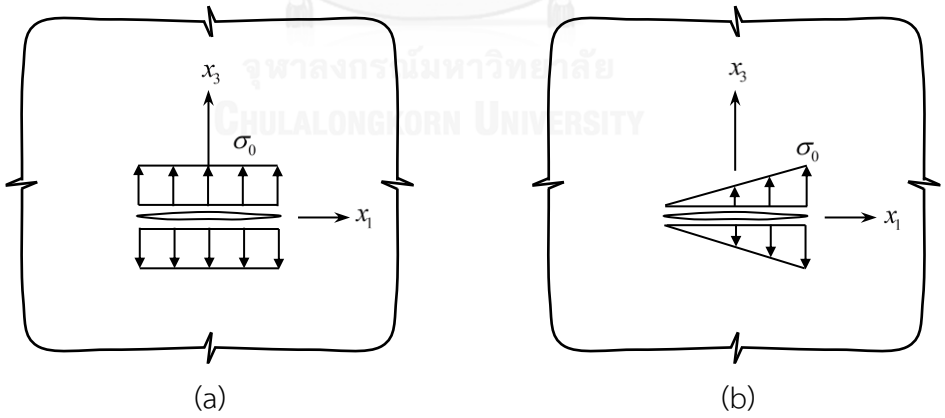

Figure 4.2 Circular crack under (a) uniformly distributed normal traction $t_3^+ = -t_3^- = \sigma_0$, and (b) linearly distributed normal traction $t_3^+ = -t_3^- = \sigma_0\left(1 + x_1/a\right)/2$

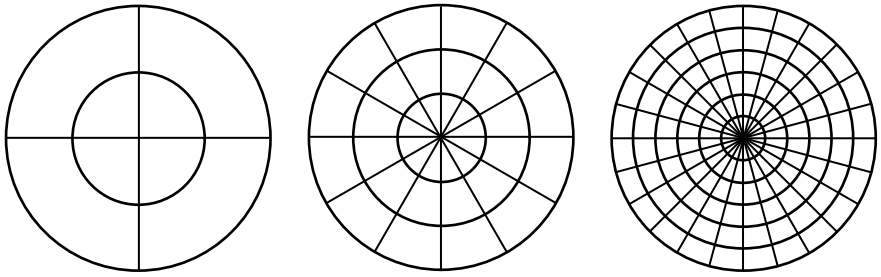

Mesh-1 Mesh-2 Mesh-3

Figure 4.3 Meshes of circular crack used in numerical study; Mesh-1 containing 8 elements and 4 crack-tip elements, Mesh-2 containing 36 elements and 12 crack-tip elements, and Mesh-3 containing 144 elements and 24 crack-tip elements

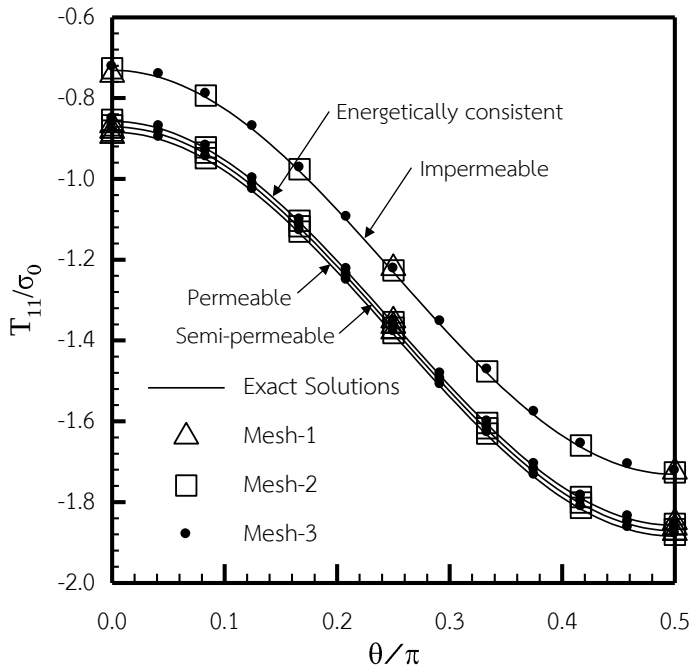

Figure 4.4 Normalized generalized T-stress component T_{11} of crack under uniform remote biaxial tension for four crack-face conditions

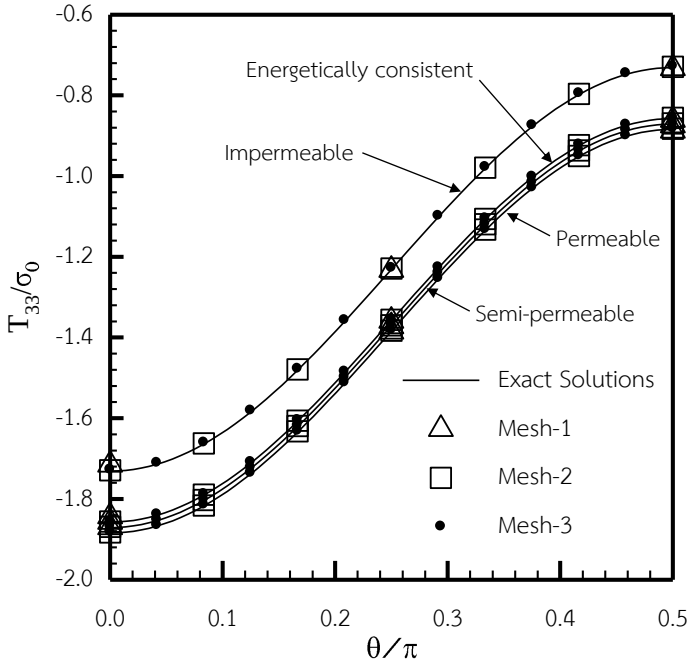

Figure 4.5 Normalized generalized T-stress component T_{33} of crack under uniform remote biaxial tension for four crack-face conditions

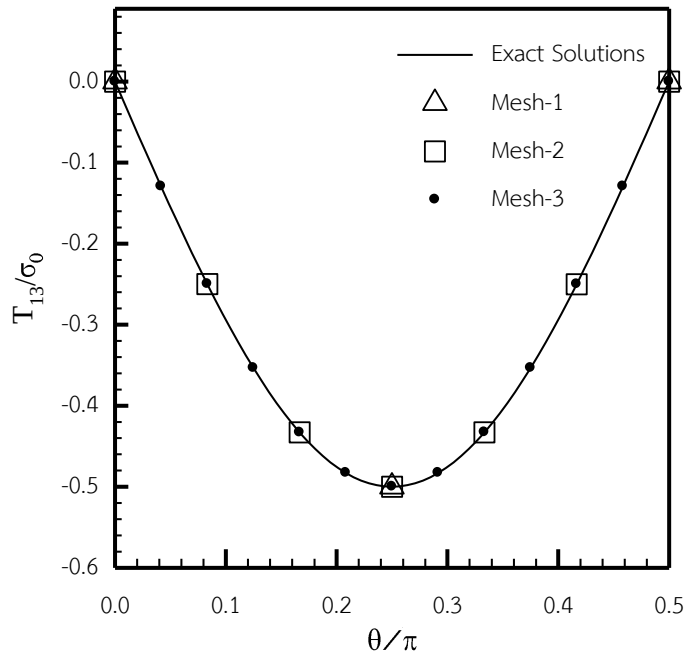

Figure 4.6 Normalized generalized T-stress component T_{13} of crack under uniform remote biaxial tension for four crack-face conditions

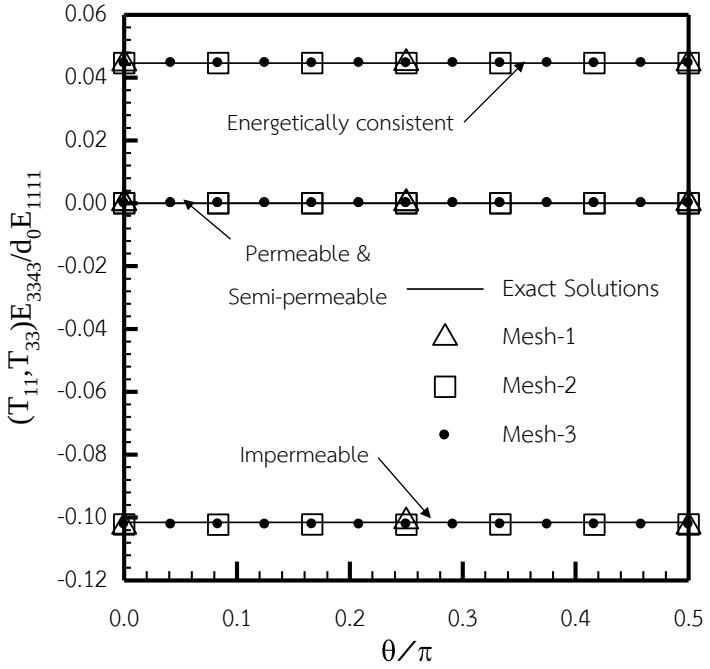

Figure 4.7 Normalized generalized T-stress components T_{11} and T_{33} of crack under uniform remote electrical induction for four crack-face conditions

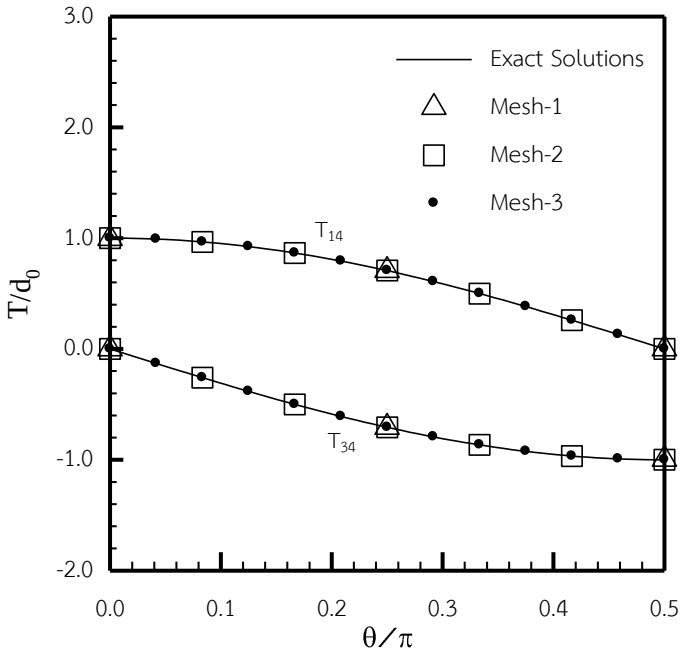

Figure 4.8 Normalized generalized T-stress components T_{14} and T_{34} of crack under uniform remote electrical induction for four crack-face conditions

4.1.3 Uniformly distributed normal traction

For the third loading case (i.e., the uniformly distributed normal traction $t_3^+ = -t_3^- = \sigma_0$), the generalized T-stress components T_{11} and T_{33} are non-zero and independent of the angular position θ due to the axisymmetry. Computed results normalized by the analytical solutions are shown in Table 4.2 for three crack-face conditions, i.e., electrically permeable, electrically impermeable and electrically semi-permeable conditions. It can be seen from these results that the computed T-stresses are in good agreement with the benchmark solutions and show slight dependence on meshes used. In particular, the errors of the predicted solutions for all three meshes are less than 0.5%.

4.1.4 Triangular distributed pressure

For the last loading case (i.e., linearly distributed normal traction $t_3^+ = -t_3^- = \sigma_0 \left(1 + x_1/a\right)/2$), only impermeable and permeable cracks are considered since there is no analytical solution for energetically consistent and electrically semi-permeable cracks. The computed generalized T-stress are reported in Figure 4.9 and 4.10 for permeable and impermeable cases, respectively. This set of results indicates that all non-zero generalized T-stress components T_{11}, T_{33} and T_{13} are dependent on the position along the crack front and, once again, the numerical results are comparable to the benchmark solutions and weakly dependent on the level of mesh refinement. In particular, results generated by the Mesh-1 differ slightly from the reference solution while results predicted by the Mesh-2 and the Mesh-3 are nearly indistinguishable from the reference solution.

Table 4.2 Normalized generalized T-stress T_{11} and T_{33} for circular crack contained in piezoelectric whole space under uniformly distributed normal traction for three crack-face conditions.

Mesh	Impermeable BC.		Permeable BC.		Semi-permeable BC.	
	$\frac{T_{11}}{T_{11}^{exact}}$	$\frac{T_{33}}{T_{33}^{exact}}$	$\frac{T_{11}}{T_{11}^{exact}}$	$\frac{T_{33}}{T_{33}^{exact}}$	$\frac{T_{11}}{T_{11}^{exact}}$	$\frac{T_{33}}{T_{33}^{exact}}$
1	0.9979	0.9984	0.9985	0.9989	0.9985	0.9989
2	0.9974	0.9988	0.9982	0.9992	0.9982	0.9992
3	0.9951	0.9980	0.9968	0.9986	0.9967	0.9986

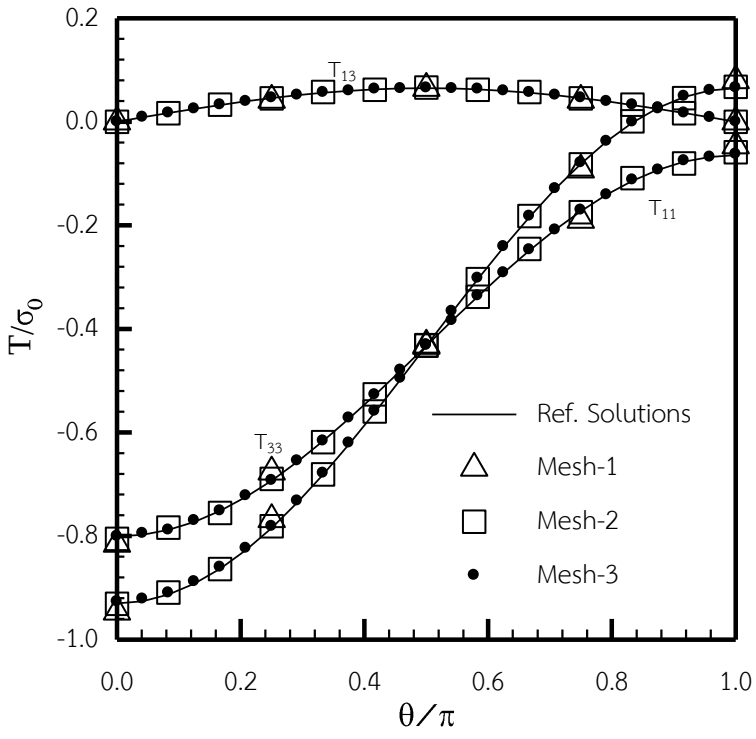

Figure 4.9 Normalized generalized T-stress components T_{11}, T_{33}, and T_{13} of impermeable crack under linearly distributed normal traction

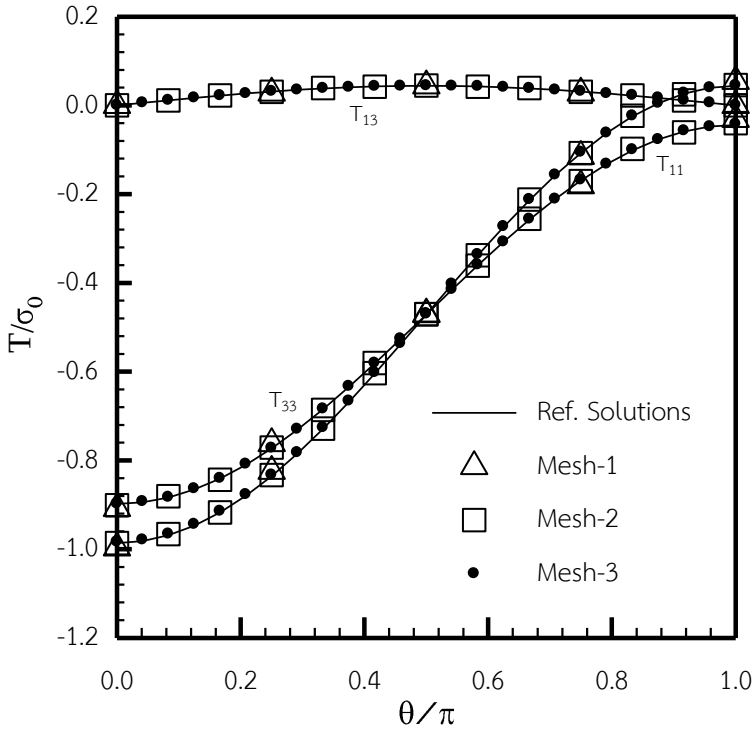

Figure 4.10 Normalized generalized T-stress components T_{11}, T_{33}, and T_{13} of permeable crack under linearly distributed normal traction

4.2 CAPABILITY OF PROPOSED TECHNIQUE

After the implemented procedure is fully verified with various benchmark cases, more complex problems are examined to further illustrate the robustness and capability of the present technique. Three representative problems, one associated with an elliptical crack, one corresponding to a spherical cap crack and the last involving a pair of identical circular cracks, are selected in the numerical study with the primary objective to show the vast feature of the present technique to model planar cracks of general geometry, non-flat cracks, and multiple cracks. Owing to the complexity of the problems consider, analytical solutions for all cases presented in this section do not exist and only the convergence of numerical results via a series of different meshes is explored. In the analysis, the permittivity of a medium filled within the crack cavity is chosen as $\kappa_c = 8.85\times10^{-12}\mathrm{C}/\left(\mathrm{Vm}\right)$ for both energetically consistent and electrically semi-permeable cracks.

4.2.1 Elliptical crack

Consider an elliptical crack contained in a linear piezoelectric whole space with a and b representing its major and minor semi-axes, respectively, as depicted in Figure 4.11(a). The poling direction and axis of material symmetry are taken along the x_3-axis whereas the crack is oriented such that the crack front is fully described by

$$x_1 = a\cos\theta\cos\beta,\ x_2 = b\sin\theta,\ x_3 = -a\cos\theta\sin\beta \tag{4.2}$$

where $\theta \in [0, 2\pi]$ denotes the angular position on the crack boundary and β denotes the angle between a normal vector to the crack surface and the x_3-axis. A body is under two loading conditions similar to the first loading cases of the previous example, i.e., the uniform remote biaxial tension $\sigma_{33}^{\infty} = 2\sigma_{11}^{\infty} = 2\sigma_0$ (also see Figure 4.11(b)) and the uniform remote electrical induction along the x_1-axis and x_3-axis $\sigma_{34}^{\infty} = 2\sigma_{14}^{\infty} = 2d_0$ (also see Figure 4.11(c)). In the analysis, the values of σ_0 and d_0 are taken as $1\times10^6\,\mathrm{N/m^2}$ and $1\times10^{-3}\,\mathrm{C/m^2}$, respectively, and the aspect ratio $a/b = 2$ and the orientation of the crack $\beta = 45^\circ$ are considered. Three meshes for a crack depicted in Figure 4.12 are adopted; in particular, the Mesh-1, the Mesh-2, and the Mesh-3 consist of 8 elements, 36 elements and 144 elements, respectively.

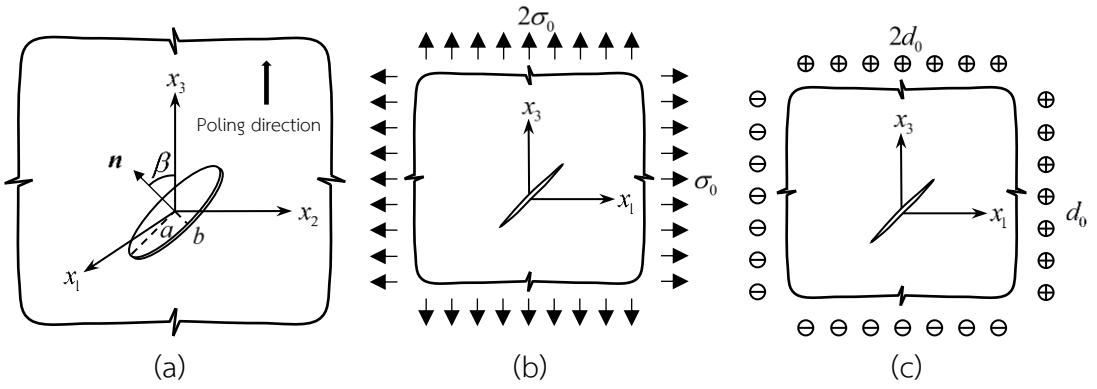

Figure 4.11 (a) Eiliptical crack in linear piezoelectric whole space, (b) body under uniform remote biaxial tension $\sigma_{33}^{\infty} = 2\sigma_{11}^{\infty} = 2\sigma_0$, and (c) body under uniform remote electrical induction $\sigma_{34}^{\infty} = 2\sigma_{14}^{\infty} = 2d_0$

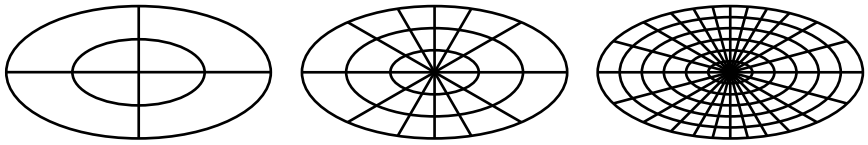

Mesh-1 Mesh-2 Mesh-3

Figure 4.12 Three meshes of elliptical crack used in the numerical study; Mesh-1 containing 8 elements and 4 crack-tip elements, Mesh-2 containing 36 elements and 12 crack-tip elements, and Mesh-3 containing 144 elements and 24 crack-tip elements

4.2.1.1 Uniform remote biaxial tension

For this loading condition, all generalized T-stress components T_{11}, T_{33}, T_{13}, T_{14} and T_{34} exist and vary along the boundary of the crack. As can be seen from results in Figures 4.13-4.17, solutions obtained from the impermeable model is notably different from those generated by other three crack-face models. In addition, numerical results show the good convergence behavior; specifically, the coarsest mesh (i.e., Mesh-1) containing relatively large elements yield results comparable to those obtained from the Mesh-2 and Mesh-3. The slight dependence on the level of refinement results directly from the use of special elements on the crack boundary to discretize the near-front relative crack-face generalized displacement.

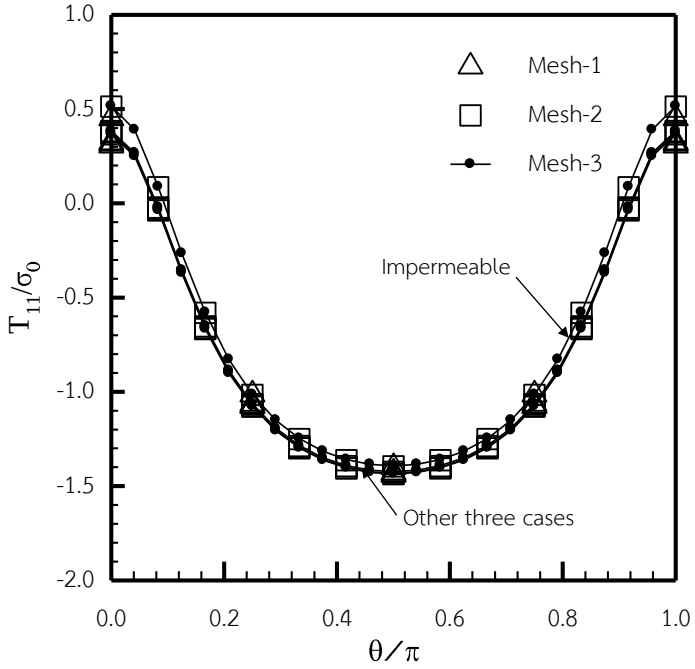

Figure 4.13 Normalized generalized T-stress component T_{11} of crack under uniform remote biaxial tension for four types of crack-face conditions

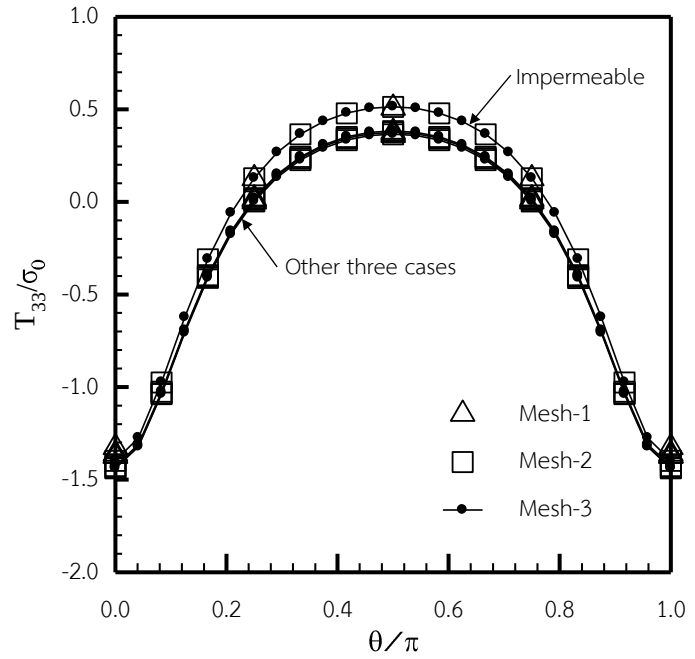

Figure 4.14 Normalized generalized T-stress component T_{33} of crack under uniform remote biaxial tension for four types of crack-face conditions

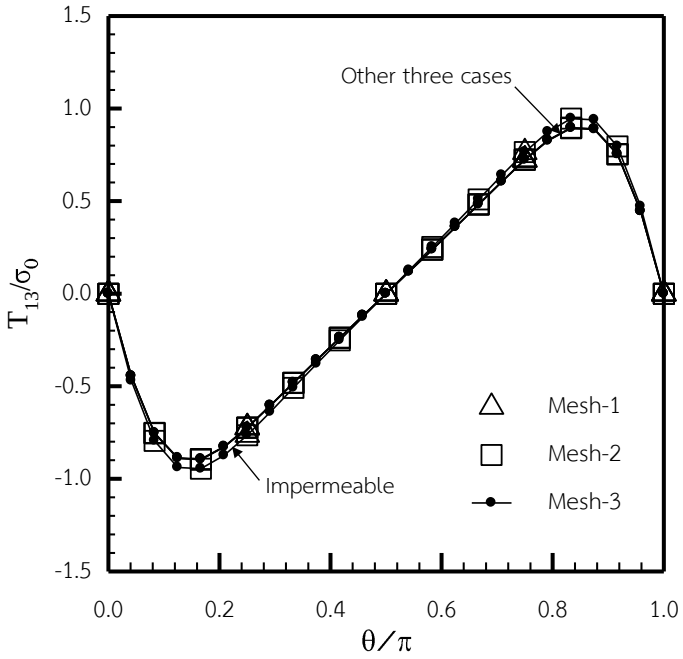

Figure 4.15 Normalized generalized T-stress component T_{13} of crack under uniform remote biaxial tension for four types of crack-face conditions

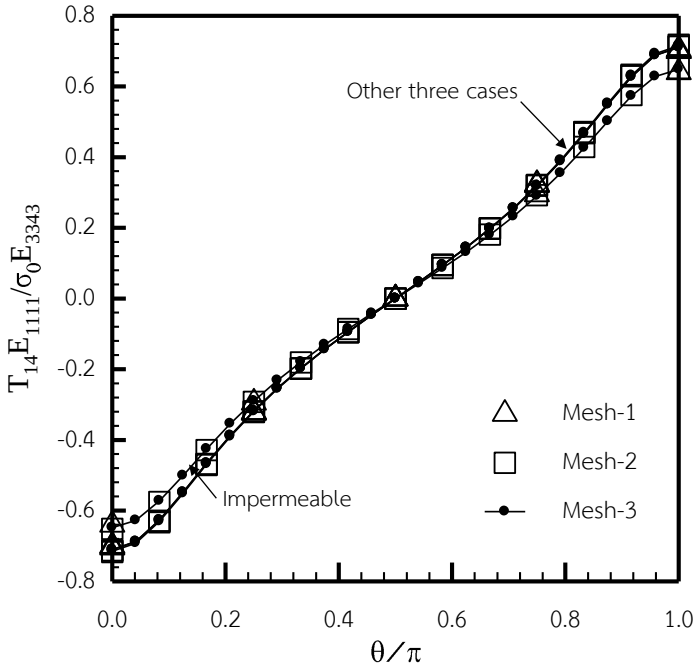

Figure 4.16 Normalized generalized T-stress component T_{14} of crack under uniform remote biaxial tension for four types of crack-face conditions

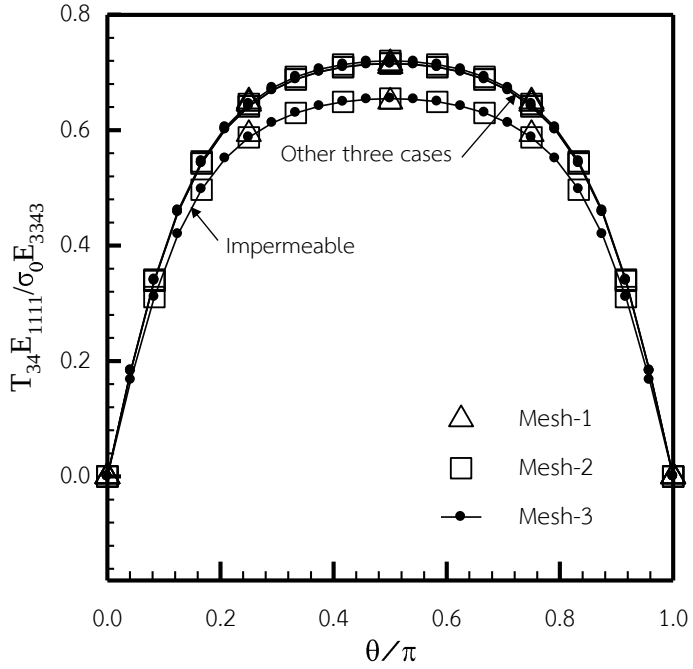

Figure 4.17 Normalized generalized T-stress component T_{34} of crack under uniform remote biaxial tension for four types of crack-face conditions

4.2.1.2 Uniform remote electric induction in the both x_1-axis and x_3-axis

For this particular loading condition, the mechanical generalized T-stress components T_{11}, T_{33} and T_{13} of permeable and semi-permeable cracks vanish whereas those associated with the other two electrically boundary conditions (i.e., impermeable and energetically consistent conditions) are non-zero and vary along the crack boundary as shown in Figure 4.18-4.20. Moreover, it can be concluded from Figure 4.21 that the computed generalized T-stress T_{14} for all four crack-face conditions are nearly identical, while the computed generalized T-stress T_{34} of the impermeable case is slightly different from those obtained from the other three crack-face conditions as clearly illustrated in Figure 4.22. Finally, it should be confirmed from numerical results shown Figure 4.18-4.22 that the present numerical procedure yields a fast rate of convergence; relatively large elements can be employed in the solution discretization.

4.2.2 Spherical cap crack

In order to treat more general crack geometry, the boundary value problem involving a non-planar crack embedded in linear piezoelectric infinite body is investigated. Consider a spherical cap crack contained in a linear piezoelectric whole space as presented in Figure 4.23(a). The surface of the crack can be parameterized by

$$x_1 = a\sin\gamma\cos\beta,\ x_2 = a\sin\gamma\sin\beta,\ x_3 = a\cos\gamma,\ \beta \in [0, 2\pi],\ \gamma \in [0, \phi] \tag{4.3}$$

where a represents the spherical crack radius; ϕ stands for the half-subtended angle of a spherical surface; and β represents an angular position along the crack front. Following four loading conditions are investigated in the numerical study: (i) the uniform remote tension in x_3-direction $\sigma_{33}^{\infty} = \sigma_0$ (see Figure 4.23(b)), (ii) the uniform remote electrical induction in x_3-direction $\sigma_{34}^{\infty} = d_0$ (see Figure 4.23(c)), (iii) the uniform remote biaxial tension $\sigma_{22}^{\infty} = 2\sigma_{11}^{\infty} = 2\sigma_0$ (see Figure 4.24(a)), and (iv) the uniform remote electrical induction along the x_1- and x_3-axes $\sigma_{24}^{\infty} = 2\sigma_{14}^{\infty} = 2d_0$ (see Figure 4.24(b)). The axis material symmetry and poling direction are taken to be coincident with the x_3-axis. In the investigation, the half subtended angle $\phi = 30^{\circ}$, $\sigma_0 = 1\times10^6 \mathrm{N/m^2}$ and $d_0 = 1\times10^{-3} \mathrm{C/m^2}$ are chosen, and three selected meshes with different levels of refinement are adopted, as illustrated in Figure 4.25, to explore the convergence characteristic of numerical solutions.

4.2.2.1 Uniform remote tension in x_3-direction

For this particular loading case, non-zero generalized T-stress components T_{11}, T_{33} and T_{14} are constant along the crack front due to the axisymmetry. The computed numerical results normalized by the benchmark solution generated by the finest mesh (i.e., Mesh-3) are reported in Table 4.3 and 4.4. It is found that the generalized T-stress components obtained from the Mesh-1 and Mesh-2 are in very good agreement with those from the finest mesh. More specifically, the difference between the results of the coarsest and intermediate meshes and those from the finest mesh all types of crack-face conditions is less than 0.4% and 0.1% for T_{11}, 0.2% and 0.02% for T_{33}, 0.4%

and 0.04% for T_{14}, respectively. In addition, the obtained results also suggest that the generalized T-stress components exhibit the strong dependence on the crack-face conditions.

4.2.2.2 Uniform remote electric induction in x_3-direction

The non-zero generalized T-stress components T_{11}, T_{33} and T_{14}, for this loading case, obtained from all three meshes are reported in Table 4.5 and 4.6. It is found that all generalized T-stress components are independent of the angular position along the crack front but they depend significantly on the boundary condition adopted on the crack surface. Moreover, it can be seen from Table 4.5 that the generalized T-stress components T_{11} and T_{33} vanishes for both electrically permeable and semi-permeable cracks but are non-zero for both impermeable and energetically consistent cracks. In addition, it can be deduced from results shown in Table 4.6 that the generalized T-stress component T_{14} is non-zero for all four crack models. Finally, it is seen from Table 4.5 and 4.6 that the computed generalized T-stress components from all meshes are in very good agreement. In particular, the discrepancy between solutions generated by the coarse and intermediate meshes and that of the fine mesh for all four crack models is less than 3.0% and 2.0% for T_{11}, 2.0% and 0.7% for T_{33}, and 0.6% and 0.8% for T_{14}, respectively.

4.2.2.3 Uniform remote biaxial tension

For the third loading condition, the non-zero generalized T-stress components T_{11}, T_{33}, T_{13}, T_{14} and T_{34} is strongly dependent on the angular position along the crack front as indicated by Figure 4.26-4.28. However, all non-zero generalized T-stress components except T_{14} are independent of crack-face boundary conditions. For the component T_{14}, solutions predicted by the electrically impermeable model appears to be slightly different from those generated by the others three crack-face conditions (see Figure 4.27). In addition, it should be remarked that the coarsest and finest meshes considered in the simulations yield results of comparable quality. This implies that the size of elements employed in the discretization slightly affect the accuracy of

numerical results and one can employ relatively coarse meshes to accurately capture the generalized T-stress along the crack front.

4.2.2.4 Uniform remote electrical induction along x_1- and x_3-axes

For the last loading condition, the generalized T-stress components T_{11}, T_{33} and T_{13} are strongly influenced by the crack-face boundary conditions as illustrated by results shown in Figures 4.29-4.31 whereas T_{34} for four crack-face conditions are nearly identical as shown in Figure 4.32. On the contrary, the crack-face condition exhibits no contribution to the value of generalized T-stress component T_{14} (see Figure 4.33). In addition, the mechanical components of the generalized traction T_{11}, T_{33} and T_{13} identically vanish for the entire crack front for both permeable and semi-permeable models. Similar to all previous loading conditions, numerical results generated by the present technique show the good convergence behavior merely slight dependence on the mesh size is observed.

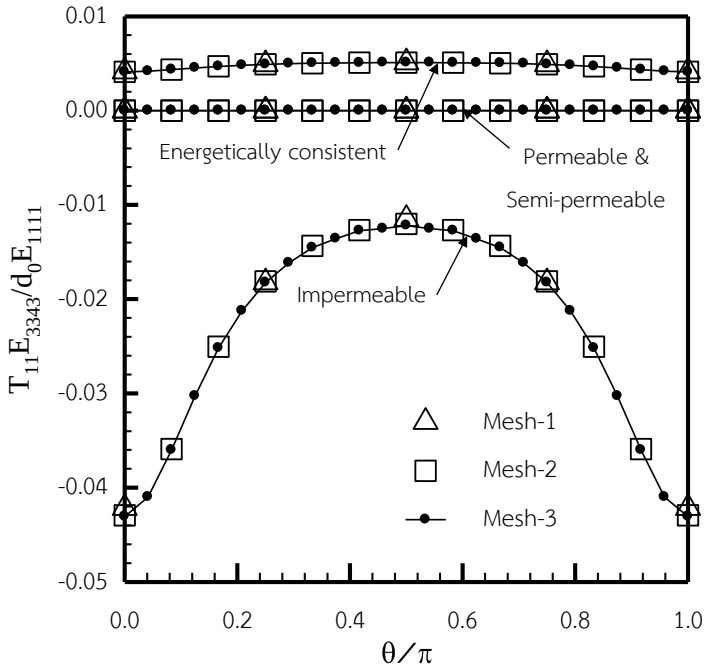

Figure 4.18 Normalized generalized T-stress component T_{11} of crack under uniform remote electrical induction for four crack-face conditions

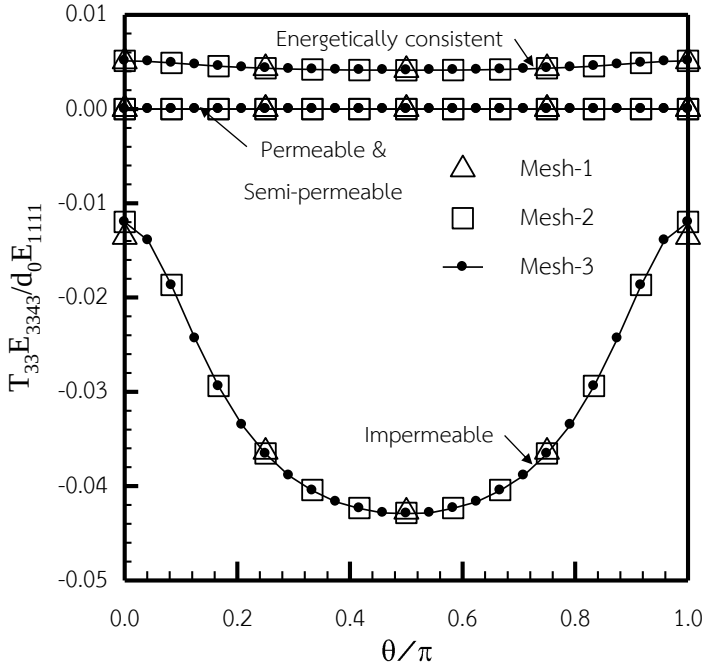

Figure 4.19 Normalized generalized T-stress component T_{33} of crack under uniform remote electrical induction for four crack-face conditions

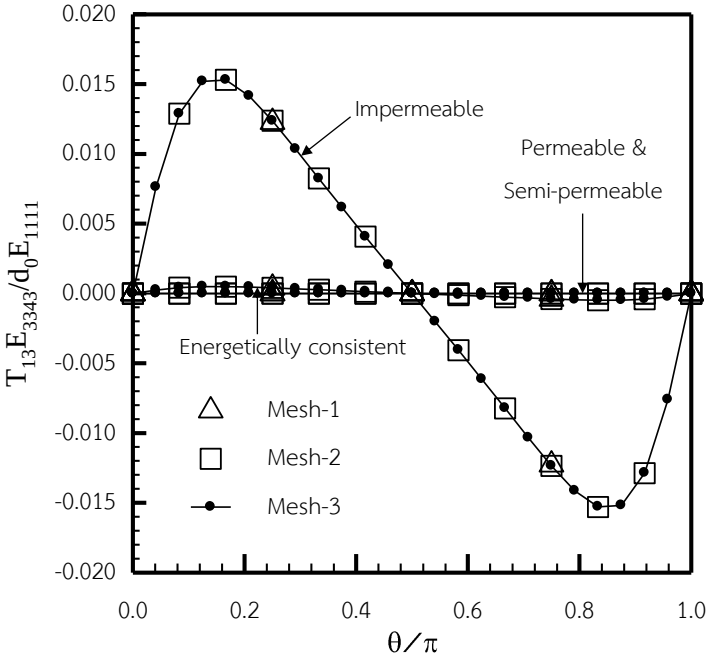

Figure 4.20 Normalized generalized T-stress component T_{13} of crack under uniform remote electrical induction for four crack-face conditions

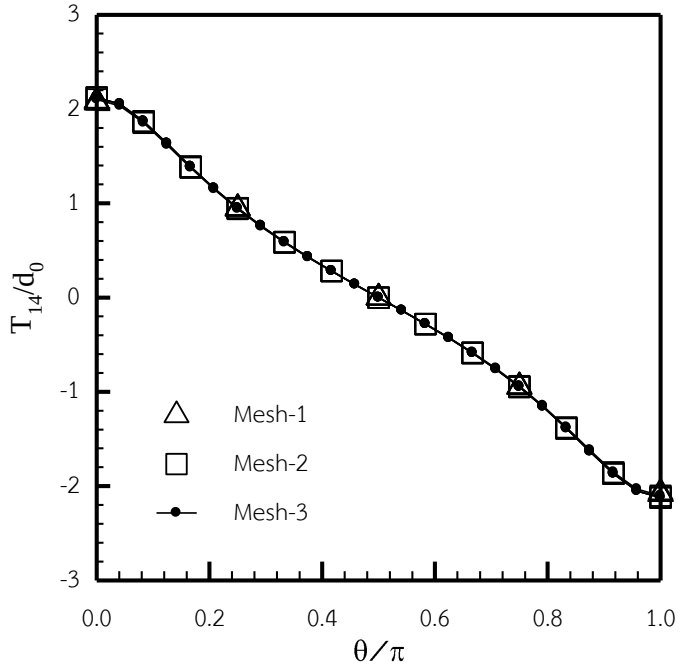

Figure 4.21 Normalized generalized T-stress component T_{14} of crack under uniform remote electrical induction for four crack-face conditions

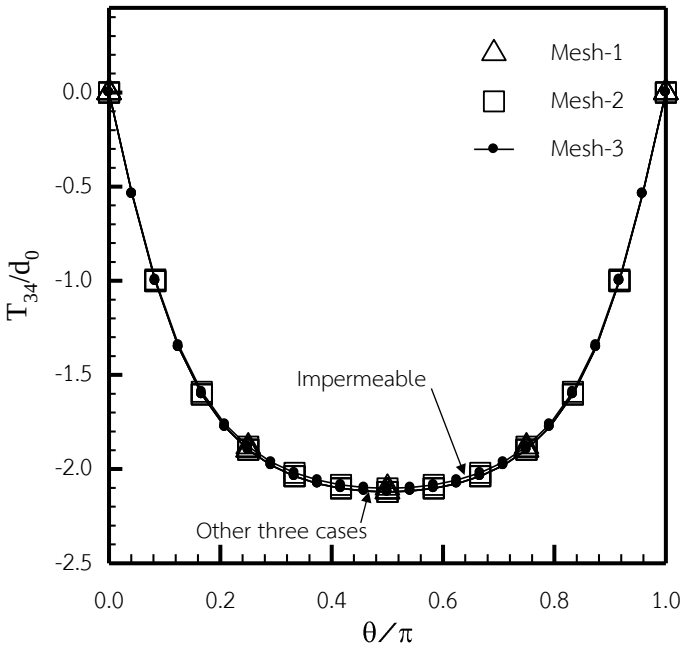

Figure 4.22 Normalized generalized T-stress component T_{34} of crack under uniform remote electrical induction for four crack-face conditions

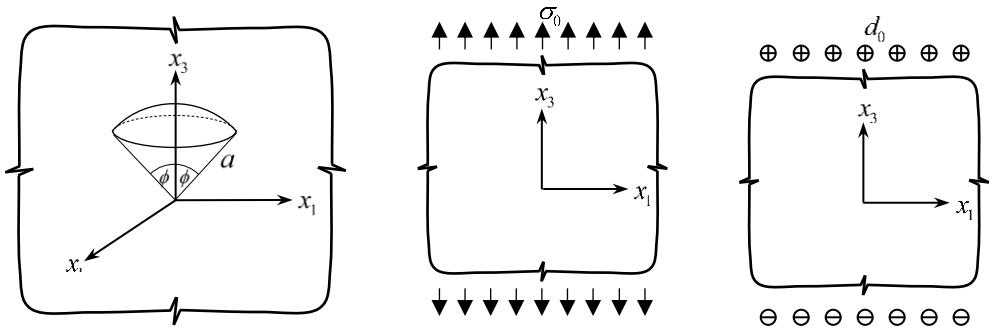

(a) (b) (c)

Figure 4.23 (a) Spherical cap crack in linear piezoelectric whole space, (b) body under uniform remote tension $\sigma_{33}^{\infty} = \sigma_0$, and (c) body under uniform remote electrical induction $\sigma_{34}^{\infty} = d_0$

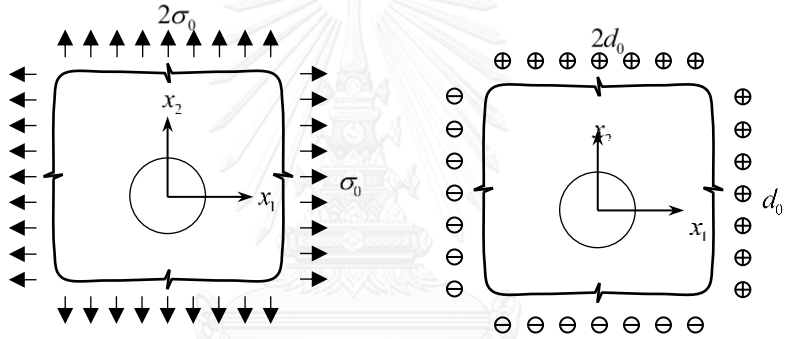

(a) (b)

Figure 4.24 Spherical cap crack in linear piezoelectric whole space under (a) uniform remote biaxial tension $\sigma_{22}^{\infty} = 2\sigma_{11}^{\infty} = 2\sigma_0$ and (b) uniform remote electrical induction $\sigma_{34}^{\infty} = 2\sigma_{14}^{\infty} = 2d_0$

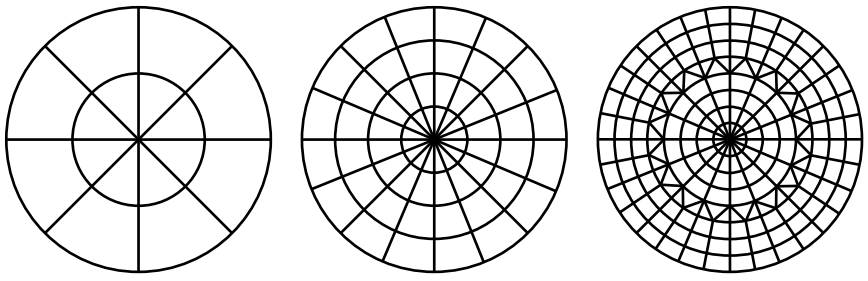

Mesh-1 Mesh-2 Mesh-3

Figure 4.25 Meshes of shperical cap crack used in numerical study; Mesh-1 containing 16 elements and 8 crack-tip elements, Mesh-2 containing 64 elements and 16 crack-tip elements, and Mesh-3 containing 288 elements and 32 crack-tip elements

Table 4.3 Normalized generalized T-stress components T_{11} and T_{33} of spherical cap crack contained in linear piezoelectric whole space under uniform remote tension for four crack-face conditions.

Mesh	Impermeable BC.		Permeable BC.		Semi-permeable BC.		Energetically consistent BC.	
	$\frac{T_{11}}{T_{11}^{ref}}$	$\frac{T_{33}}{T_{33}^{ref}}$	$\frac{T_{11}}{T_{11}^{ref}}$	$\frac{T_{33}}{T_{33}^{ref}}$	$\frac{T_{11}}{T_{11}^{ref}}$	$\frac{T_{33}}{T_{33}^{ref}}$	$\frac{T_{11}}{T_{11}^{ref}}$	$\frac{T_{33}}{T_{33}^{ref}}$
1	0.9998	0.9994	0.9966	0.9989	0.9969	0.9989	0.9968	0.9989
2	1.0008	1.0001	0.9994	0.9998	0.9996	0.9998	0.9995	0.9998
3	1.0000	1.0000	1.0000	1.0000	1.0000	1.0000	1.0000	1.0000

Table 4.4 Normalized generalized T-stress component T_{14} of spherical cap crack contained in linear piezoelectric whole space under uniform remote tension for four crack-face conditions.

Mesh	Impermeable BC.	Permeable BC.	Semi-permeable BC.	Energetically consistent BC.
	$\frac{T_{14}}{T_{14}^{ref}}$	$\frac{T_{14}}{T_{14}^{ref}}$	$\frac{T_{14}}{T_{14}^{ref}}$	$\frac{T_{14}}{T_{14}^{ref}}$
1	0.9965	0.9963	0.9962	0.9961
2	1.0001	0.9996	0.9996	0.9996
3	1.0000	1.0000	1.0000	1.0000

Table 4.5 Normalized generalized T-stress components T_{11} and T_{33} of spherical cap crack contained in linear piezoelectric whole space under uniform remote electrical induction for four crack-face conditions.

Mesh	Impermeable BC.		Permeable BC.		Semi-permeable BC.		Energetically consistent BC.	
	$\frac{T_{11}}{T_{11}^{ref}}$	$\frac{T_{33}}{T_{33}^{ref}}$	$\frac{T_{11}E_{3343}}{d_0E_{1111}}$	$\frac{T_{33}E_{3343}}{d_0E_{1111}}$	$\frac{T_{11}E_{3343}}{d_0E_{1111}}$	$\frac{T_{33}E_{3343}}{d_0E_{1111}}$	$\frac{T_{11}}{T_{11}^{ref}}$	$\frac{T_{33}}{T_{33}^{ref}}$
1	0.9720	0.9872	0.0000	0.0000	0.0000	0.0000	1.0112	1.0073
2	0.9886	0.9935	0.0000	0.0000	0.0000	0.0000	1.0012	1.0004
3	1.0000	1.0000	0.0000	0.0000	0.0000	0.0000	1.0000	1.0000

Table 4.6 Normalized generalized T-stress component T_{14} of spherical cap crack contained in linear piezoelectric whole space under uniform remote electrical induction for four crack-face conditions.

Mesh	Impermeable BC.	Permeable BC.	Semi-permeable BC.	Energetically consistent BC.
	$\frac{T_{14}}{T_{14}^{ref}}$	$\frac{T_{14}}{T_{14}^{ref}}$	$\frac{T_{14}}{T_{14}^{ref}}$	$\frac{T_{14}}{T_{14}^{ref}}$
1	1.0006	0.9994	0.9994	0.9998
2	1.0008	1.0001	1.0001	1.0001
3	1.0000	1.0000	1.0000	1.0000

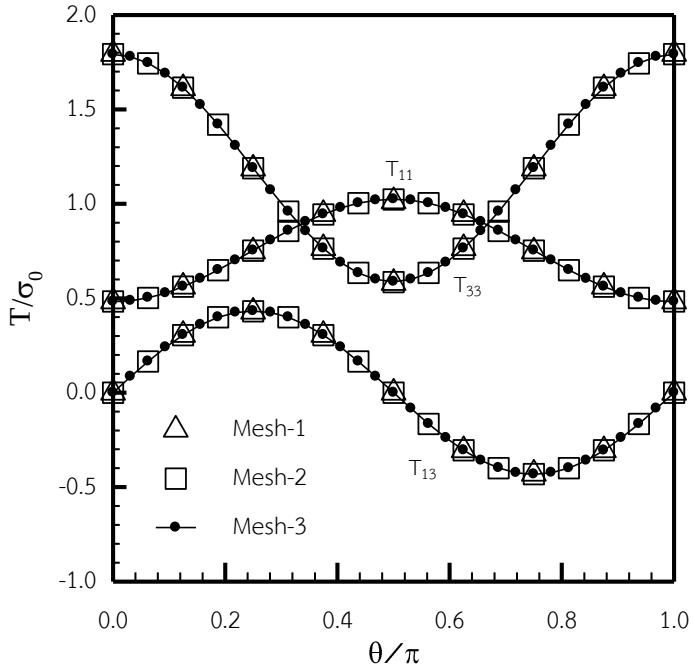

Figure 4.26 Normalized generalized T-stress components T_{11}, T_{33} and T_{13} of crack under uniform remote biaxial tension for four crack-face conditions

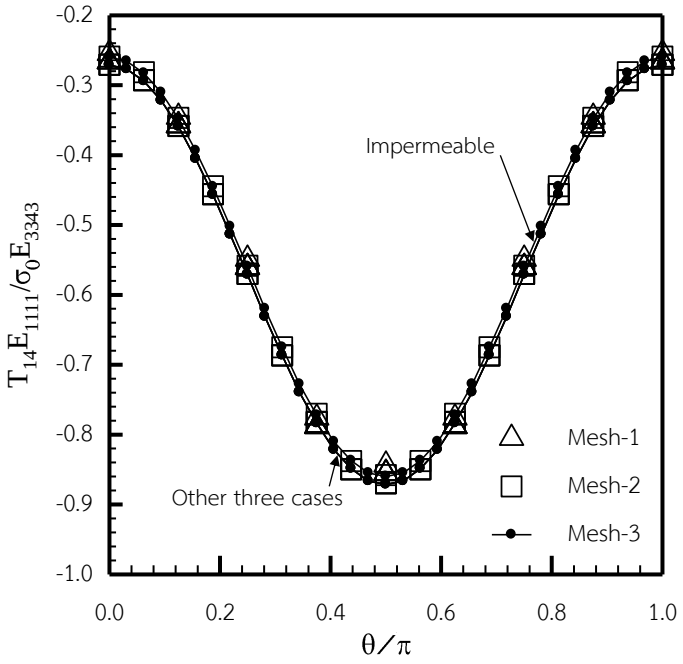

Figure 4.27 Normalized generalized T-stress component T_{14} of crack under uniform remote biaxial tension for four crack-face conditions

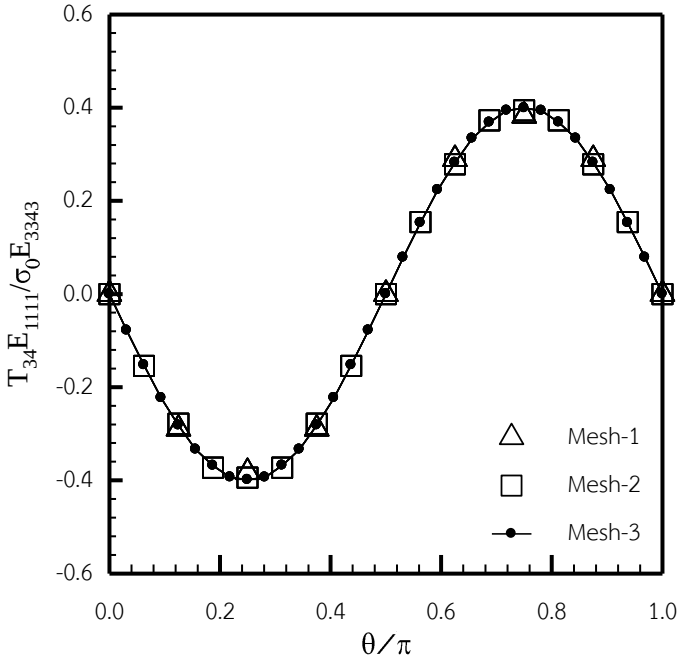

Figure 4.28 Normalized generalized T-stress component T_{34} of crack under uniform remote biaxial tension for four crack-face conditions

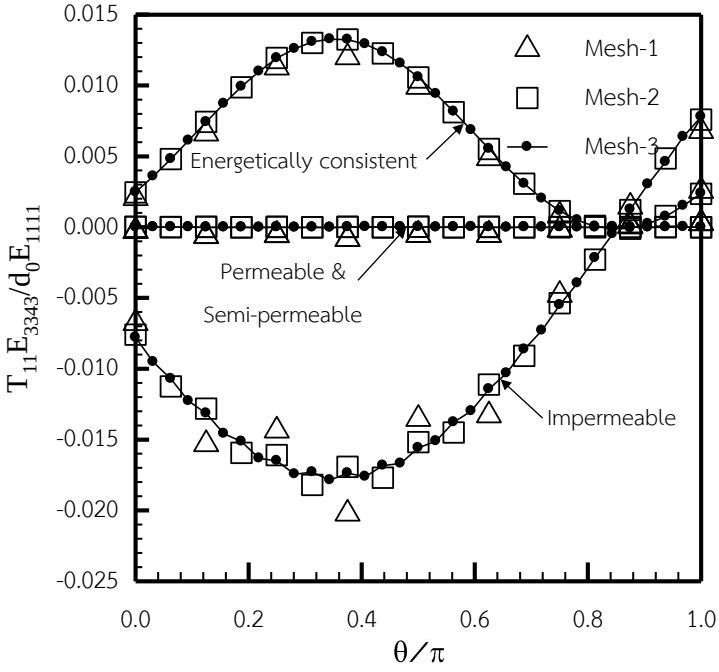

Figure 4.29 Normalized generalized T-stress component T_{11} of crack under uniform remote electrical induction for four crack-face conditions

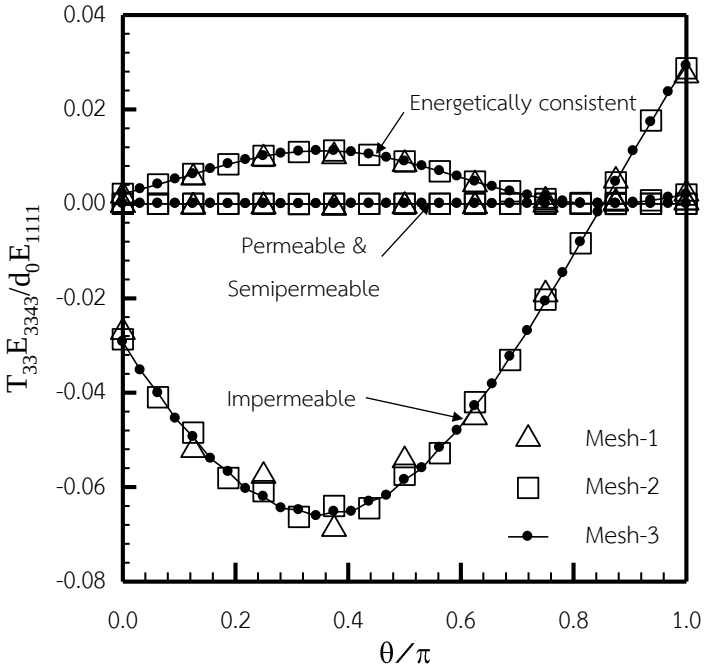

Figure 4.30 Normalized generalized T-stress component T_{33} of crack under uniform remote electrical induction for four crack-face conditions

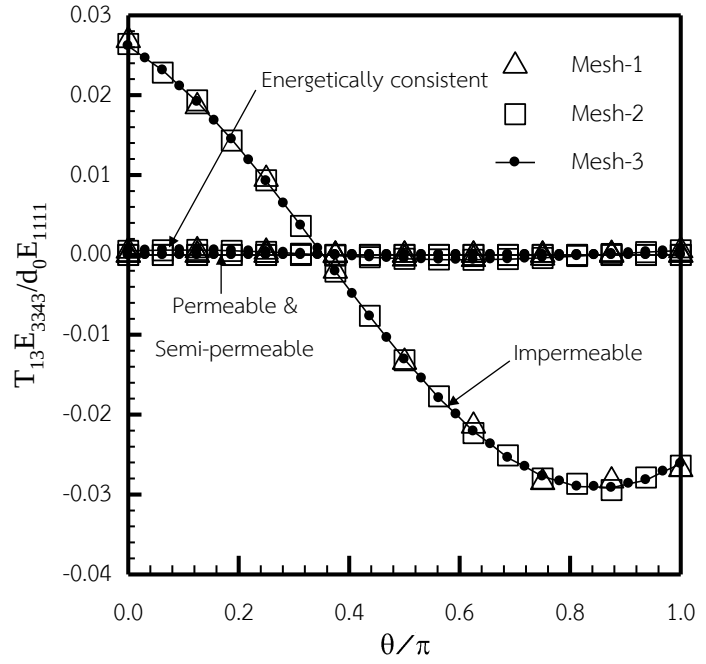

Figure 4.31 Normalized generalized T-stress component T_{13} of crack under uniform remote electrical induction for four crack-face conditions

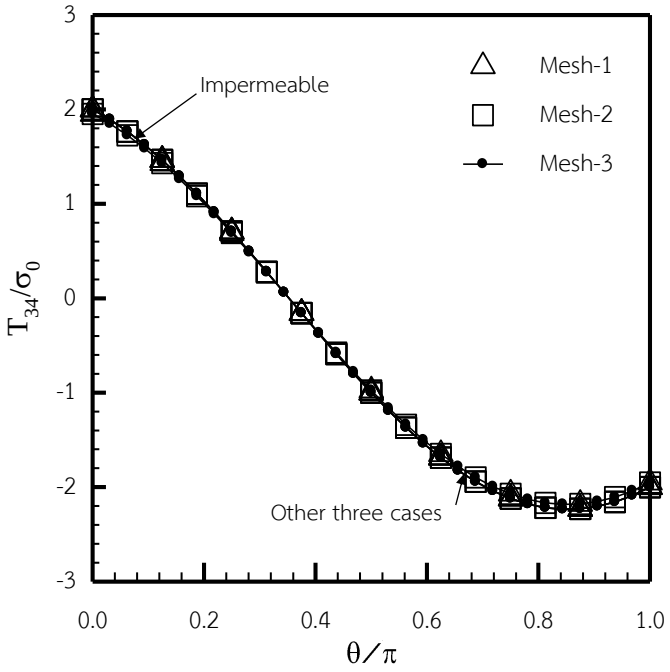

Figure 4.32 Normalized generalized T-stress component T_{34} of crack under uniform remote electrical induction for four crack-face conditions

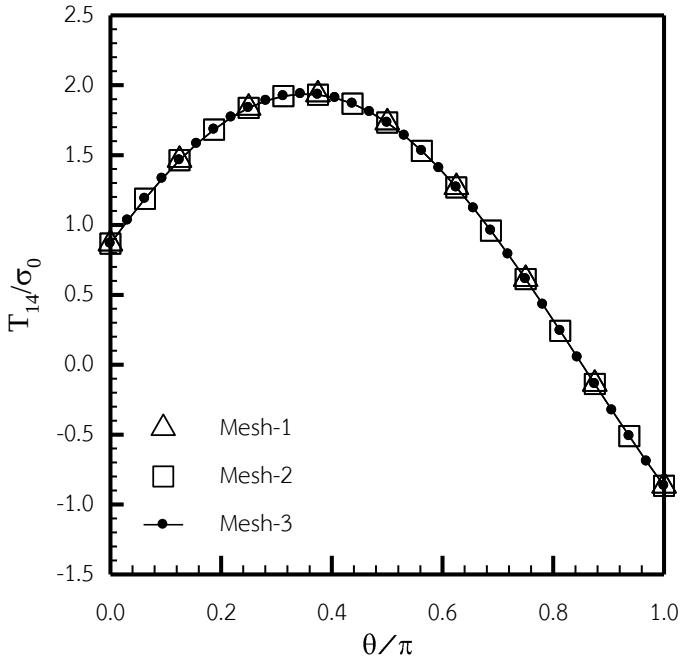

Figure 4.33 Normalized generalized T-stress component T_{14} of crack under uniform remote electrical induction for four crack-face conditions

4.2.3 A pair of identical circular cracks

As the last example, consider a pair of identical circular cracks with the radius a contained in a linear piezoelectric whole space as illustrated in Figure 4.34. The two cracks, called crack-A and crack-B, are oriented such that their centers are located at the points $(0,0,-d)$ and $(0,0,d)$, respectively, and the crack surface is normal to the x_3-axis. The medium is subjected to two loading conditions, one for the uniform uniaxial remote stress in the x_3-direction $\sigma_{33}^{\infty}=\sigma_0$ (see Figure 4.34(a)) and the other for the uniform electrical induction in the x_3-direction $\sigma_{34}^{\infty}=d_0$ (see Figure 4.34(b)). In the analysis, $d/a=0.25$, $\sigma_0=1\times10^6\,\mathrm{N/m^2}$ and $d_0=1\times10^{-3}\,\mathrm{C/m^2}$ are considered and three meshes shown in Figure 4.3 are employed to discretize both cracks.

Computed generalized T-stress components for the crack-A are normalized by the single crack solution and then reported in Figure 4.7 and 4.8 for both loading conditions. It is remarked that it is sufficient to present only results of the crack-A due to the symmetry and the normalization by the single crack solution is only for demonstrating the effect of the interaction between the two cracks. It can be seen from these results that the convergence of numerical results is achieved as the level of discretization is refined. Specifically, the coarsest mesh yields results with only slight difference from those from the finest mesh. It is also found that for the second loading case, the mechanical generalized T-stress components T_{11} and T_{33} vanishes for both electrically permeable and electrically semi-permeable crack-face conditions. This finding is similar to that observed in a single penny-shaped crack.

To further investigate the influence of interacting cracks, results of the generalized T-stress components for different values of d/a are computed by using the Mesh-3. The obtained results for T_{11}, T_{33} and T_{14} are reported along with the single-crack solution as shown in Figures 4.35-4.37, respectively. Results from those Figures indicate that decreasing the normalized distance d/a enhances the interaction between the two cracks. On the contrary, as d/a increases, solutions of the two cracks converge rapidly to results of a single crack. It is important to note that as the ratio d/a increases, the magnitude of T_{11} and T_{33} increases rapidly to reach the maximum

value and then decreases monotonically to the single-crack solution whereas the magnitude of T_{14} increases monotonically and converges to the single-crack solution.

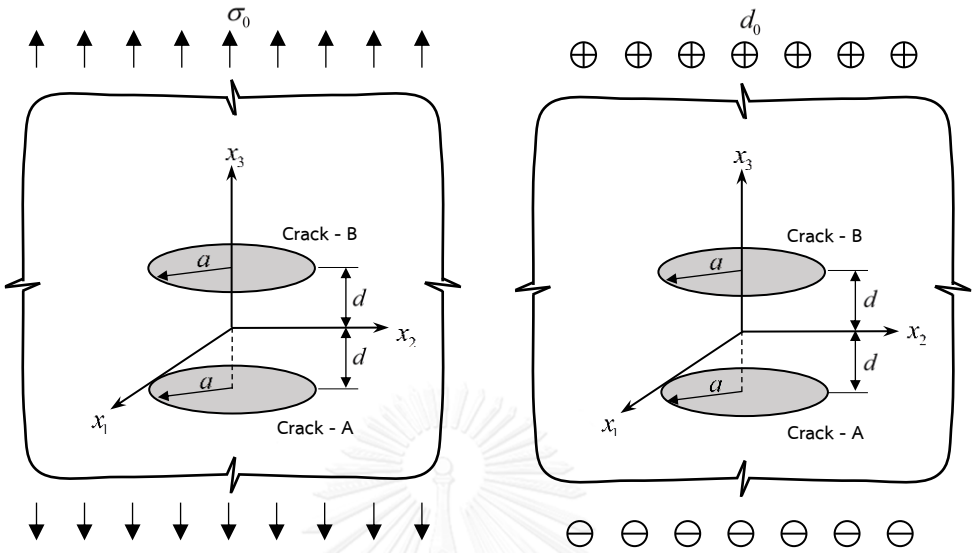

Figure 4.34 Schematic of a pair of identical circular cracks under (a) uniform uniaxial remote stress σ_0 in x_3-direction (b) uniform remote electrical induction d_0 in x_3-direction

Table 4.7 Normalized generalized T-stress components T_{11} and T_{33} of a pair of circular cracks in linear piezoelectric whole space under uniform uniaxial remote stress in x_3-direction for four rack-face conditions.

Mesh	Impermeable BC.		Permeable BC.		Semi-permeable BC.		Energetically consistent BC.	
	$\frac{T_{11}}{T_{11}^{ref}}$	$\frac{T_{33}}{T_{33}^{ref}}$	$\frac{T_{11}}{T_{11}^{ref}}$	$\frac{T_{33}}{T_{33}^{ref}}$	$\frac{T_{11}}{T_{11}^{ref}}$	$\frac{T_{33}}{T_{33}^{ref}}$	$\frac{T_{11}}{T_{11}^{ref}}$	$\frac{T_{33}}{T_{33}^{ref}}$
1	1.0258	0.8423	1.0245	0.8567	1.0247	0.8555	1.0247	0.8555
2	1.0669	0.8608	1.0625	0.8737	1.0631	0.8727	1.0631	0.8727
3	1.0799	0.8665	1.0748	0.8790	1.0755	0.8781	1.0755	0.8781

Table 4.8 Normalized generalized T-stress T_{11} and T_{33} of a pair of circular cracks in linear piezoelectric whole space under uniform remote electrical induction in x_3-direction for four crack-face conditions.

Mesh	Impermeable BC.		Permeable BC.		Semi-permeable BC.		Energetically consistent BC.	
	$\frac{T_{11}}{T_{11}^{ref}}$	$\frac{T_{33}}{T_{33}^{ref}}$	$\frac{T_{11}E_{3343}}{d_0E_{1111}}$	$\frac{T_{33}E_{3343}}{d_0E_{1111}}$	$\frac{T_{11}E_{3343}}{d_0E_{1111}}$	$\frac{T_{33}E_{3343}}{d_0E_{1111}}$	$\frac{T_{11}}{T_{11}^{ref}}$	$\frac{T_{33}}{T_{33}^{ref}}$
1	1.0080	1.0116	0.0000	0.0000	0.0000	0.0000	1.0234	0.8613
2	1.0140	1.0122	0.0000	0.0000	0.0000	0.0000	1.0601	0.8776
3	1.0205	1.0146	0.0000	0.0000	0.0000	0.0000	1.0717	0.8825

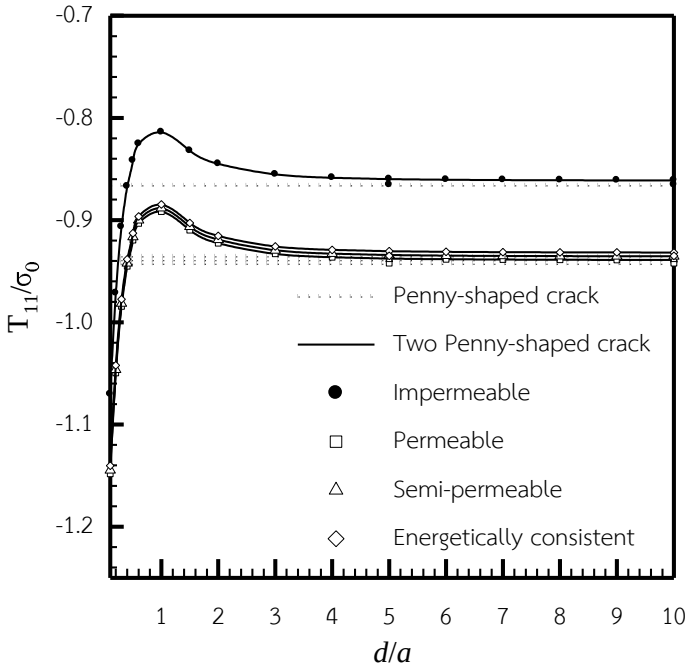

Figure 4.35 Normalized generalized T-stress component T_{11} of crack under uniform remote tension for four crack-face conditions

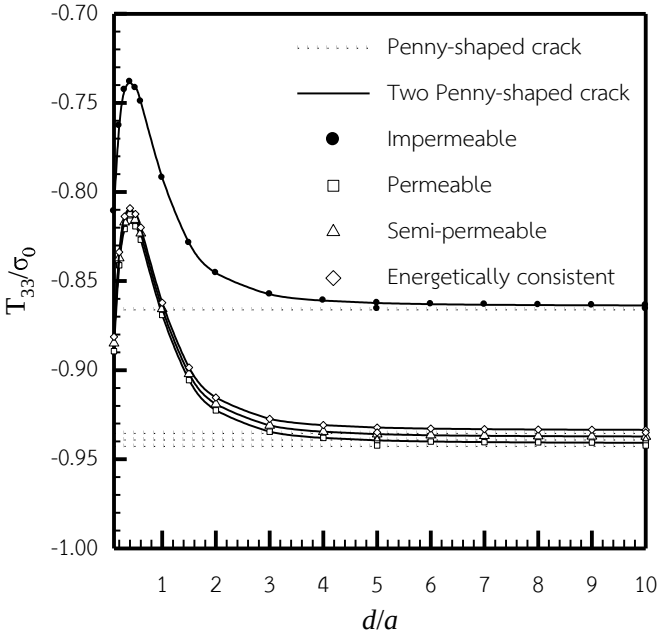

Figure 4.36 Normalized generalized T-stress component T_{33} of crack under uniform remote tension for four crack-face conditions

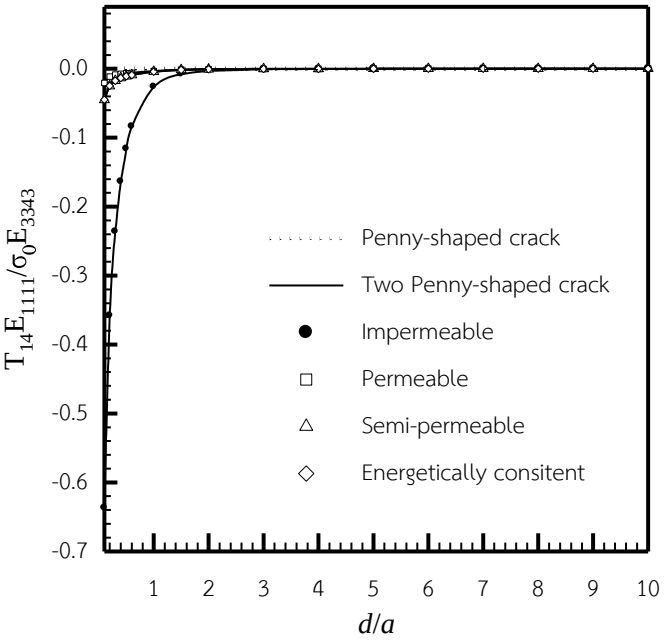

Figure 4.37 Normalized generalized T-stress component T_{14} of crack under uniform remote tension for four crack-face conditions

CHAPTER 5
CONCLUSIONS AND REMARKS

An accurate and efficient numerical procedure based upon the weakly singular, boundary integral equation method and standard Galerkin technique for analysis of generalized T-stress components of general cracks in three-dimensional, linear piezoelectric, whole space under various crack-face conditions has been successfully developed. The technique has been implemented in a general framework allowing planar, non-planar and multiple cracks in generally anisotropic piezoelectric medium under arbitrarily distributed applied crack-face loadings and uniform mechanical and electrical fields to be treated. A pair of weakly singular, weak-form integral equations, one for the sum of the crack-face generalized displacement and the other for the jump in the crack-face generalized traction, has been developed and employed in the formulation of key equations governing the unknown on the crack surface. The weak-form boundary integral equations are fully regularized and contain merely the weakly singular kernels. As a result, it makes all involved integrals existing in the sense of Riemann and their validity only needs the continuity of the crack-face data. In addition, the weakly singular nature of the boundary integral equations also eases their interpretation and numerical evaluation in comparison with strongly singular and hypersingular integrals commonly involved in conventional boundary integral equation methods.

The weakly singular boundary element method together with the standard Galerkin scheme is utilized to discretize both a pair of weakly singular integral equations and the energetically consistent and electrically semi-permeable crack-face conditions. To enhance the quality of solution approximation and computational efficiency, special local basis functions have been employed to approximate the near-front jump in the crack-face generalized displacement; the special quadrature has been utilized to treat both weakly singular and near singular double surface integrals; and an interpolation scheme has been implemented to compute kernels for general anisotropic piezoelectric materials. The discretization of a pair of boundary integral equations yields two systems of linear algebraic equations whereas that of the

prescribed energetically consistent and electrically semi-permeable crack-face conditions leads to two systems of nonlinear algebraic equations. All involved sets of linear algebraic equations are solved by a preconditioning conjugate gradient method whereas the resulting set of nonlinear equations (for the case of energetically consistent and electrically semi-permeable cracks) is solved by a nonlinear solver based on Newton iteration.

After all crack-face unknowns data are solved, the generalized T-stress components along the crack front have been post-processed using the information of the sum of the crack-face generalized displacement and the known crack-face generalized traction in the limiting point of the crack boundary. Results from extensive numerical experiments for various scenarios (e.g., planar and nonplanar cracks, multiple cracks, cracks under general loading conditions) have indicated that the proposed technique is computationally robust and, in addition, gives very accurate results in comparison with available benchmark solution with use of reasonably coarse meshes.

Finally, it is remarked that the formulation and implementations are still limited to cracks in an infinite medium. The extension of the present development to simulate cracks in a finite body should be potentially useful for modeling more practical and large-scale problems. All components established in this current investigation should at least provide an essential basis for such generalization.

REFERENCES

Chen, M.-C. (2003). Application of finite-part integrals to three-dimensional fracture problems for piezoelectric media Part I: Hypersingular integral equation and theoretical analysis. *International journal of fracture, 121*(3-4), 133-148.

Chen, W., & Lim, C. (2005). 3D point force solution for a permeable penny-shaped crack embedded in an infinite transversely isotropic piezoelectric medium. *International journal of fracture, 131*(3), 231-246.

Chen, W., & Shioya, T. (2000). Complete and exact solutions of a penny-shaped crack in a piezoelectric solid: antisymmetric shear loadings. *International Journal of Solids and Structures, 37*(18), 2603-2619.

Chen, W., Shioya, T., & Ding, H. (2000). A penny-shaped crack in piezoelectrics: resolved. *International journal of fracture, 105*(1), 49-56.

Chiang, C.-R., & Weng, G. J. (2007). Nonlinear behavior and critical state of a penny-shaped dielectric crack in a piezoelectric solid. *Journal of Applied Mechanics, 74*(5), 852-860.

Davì, G., & Milazzo, A. (2001). Multidomain boundary integral formulation for piezoelectric materials fracture mechanics. *International Journal of Solids and Structures, 38*(40), 7065-7078.

Groh, U., & Kuna, M. (2005). Efficient boundary element analysis of cracks in 2D piezoelectric structures. *International Journal of Solids and Structures, 42*(8), 2399-2416.

Hao, M., & Biao, W. (2004). T-stress in piezoelectric solid. *Applied Mathematics and Mechanics, 25*(5), 513-517.

Lee, D.-J., Shin, D.-C., Cho, Y., & Watanabe, K. (2011). A study of the effect of the electro-mechanical loading history on the fracture strength of piezoelectric material. *Engineering Fracture Mechanics, 78*(7), 1374-1388.

Li, Q., Ricoeur, A., & Kuna, M. (2011). Coulomb traction on a penny-shaped crack in a three dimensional piezoelectric body. *Archive of Applied Mechanics, 81*(6), 685-700.

Liu, S., Shen, Y., & Liu, J. (2012). Exact solutions for piezoelectric materials with an elliptic hole or a crack under uniform internal pressure. *Chinese Journal of Mechanical Engineering, 25*(4), 845-852.

Okayasu, M., Ozeki, G., & Mizuno, M. (2010). Fatigue failure characteristics of lead zirconate titanate piezoelectric ceramics. *Journal of the European Ceramic Society, 30*(3), 713-725.

Pan, E. (1999). A BEM analysis of fracture mechanics in 2D anisotropic piezoelectric solids. *Engineering Analysis with Boundary Elements, 23*(1), 67-76.

Park, S., & Sun, C. (1993). Effect of electric field on fracture of piezoelectric ceramics. *International journal of fracture, 70*(3), 203-216.

Phongtinnaboot, W., Rungamornrat, J., & Chintanapakdee, C. (2011). Modeling of cracks in 3D piezoelectric finite media by weakly singular SGBEM. *Engineering Analysis with Boundary Elements, 35*(3), 319-329.

Pich, V. C., Phongtinnaboot, W., & Rungamornrat, J. (2015). *Analytical Solutions of Generalized T-stresses for Impermeable and Permeable Penny-shaped Cracks in Linear Piezoelectric Media*. Paper presented at the The Twenty-Eight KKHTCNN Symposium on Civil Engineering Bangkok, Thailand.

Qin, T., Yu, Y., & Noda, N. (2007). Finite-part integral and boundary element method to solve three-dimensional crack problems in piezoelectric materials. *International Journal of Solids and Structures, 44*(14), 4770-4783.

Rajapakse, R., & Xu, X.-L. (2001). Boundary element modeling of cracks in piezoelectric solids. *Engineering Analysis with Boundary Elements, 25*(9), 771-781.

Rungamornrat, J., & Mear, M. E. (2008a). Analysis of fractures in 3D piezoelectric media by a weakly singular integral equation method. *International journal of fracture, 151*(1), 1-27.

Rungamornrat, J., & Mear, M. E. (2008b). Weakly-singular, weak-form integral equations for cracks in three-dimensional anisotropic media. *International Journal of Solids and Structures, 45*(5), 1283-1301.

Rungamornrat, J., Phongtinnaboot, W., & Wijeyewickrema, A. (2015). Analysis of cracks in 3D piezoelectric media with various electrical boundary conditions. *International journal of fracture, 192*(2), 133-153.

Rungamornrat, J., & Senjuntichai, T. (2009). Regularized boundary integral representations for dislocations and cracks in smart media. *Smart Materials and Structures, 18*(7), 074010.

Sanz, J., Ariza, M., & Dominguez, J. (2005). Three-dimensional BEM for piezoelectric fracture analysis. *Engineering Analysis with Boundary Elements, 29*(6), 586-596.

Shindo, Y., Narita, F., & Saito, F. (2007). Static fatigue behavior of cracked piezoelectric ceramics in three-point bending under electric fields. *Journal of the European Ceramic Society, 27*(10), 3135-3140.

Solis, M., Sanz, J., Ariza, M., & Dominguez, J. (2009). Analysis of cracked piezoelectric solids by a mixed three-dimensional BE approach. *Engineering Analysis with Boundary Elements, 33*(3), 271-282.

Subsathaphol, T. (2013). *Analysis of T-stress for cracks in 3D linear piezoelectric media.* (Master Degree), Chulalongkorn University.

Subsathaphol, T., Rungamornrat, J., & Phongtinnaboot, W. (2014, May 14-16). *Analysis of generalized T-stress for cracks in 3D linear piezoelectric media.* Paper presented at the National Convention on Civil Engineering, Pullman Hotel, Khon Kaen.

Viola, E., Boldrini, C., & Tornabene, F. (2008). Non-singular term effect on the fracture quantities of a crack in a piezoelectric medium. *Engineering Fracture Mechanics, 75*(15), 4542-4567.

Wang, B., & Mai, Y.-W. (2003). On the electrical boundary conditions on the crack surfaces in piezoelectric ceramics. *International Journal of Engineering Science, 41*(6), 633-652.

Wang, X., & Jiang, L. (2002). *Fracture behaviour of cracks in piezoelectric media with electromechanically coupled boundary conditions.* Paper presented at the Proceedings of the Royal Society of London A: Mathematical, Physical and Engineering Sciences.

Wippler, K., & Kuna, M. (2007). Crack analyses in three-dimensional piezoelectric structures by the BEM. *Computational materials science, 39*(1), 261-266.

Xu, X.-L., & Rajapakse, R. (1999). Analytical solution for an arbitrarily oriented void/crack and fracture of piezoceramics. *Acta materialia, 47*(6), 1735-1747.

Xu, X.-L., & Rajapakse, R. (2001). On a plane crack in piezoelectric solids. *International Journal of Solids and Structures, 38*(42), 7643-7658.

Zhao, M.-H., Fang, P.-Z., & Shen, Y.-P. (2004). Boundary integral–differential equations and boundary element method for interfacial cracks in three-dimensional piezoelectric media. *Engineering Analysis with Boundary Elements, 28*(7), 753-762.

Zhong, X.-C., & Li, X.-F. (2008). T-stress analysis for a Griffith crack in a magnetoelectroelastic solid. *Archive of Applied Mechanics, 78*(2), 117-125.

Zhu, T., & Yang, W. (1999). Crack kinking in a piezoelectric solid. *International Journal of Solids and Structures, 36*(33), 5013-5027.

APPENDIX

VITA

Varuj Limwibul was born on April 19, 1992 in Bangkok, Thailand, the son of Somkit Limwibul and Vantana Limwibul. He graduated Bachelor of Engineering degree in Civil Engineering program from Chulalongkorn University in 2014. In 2015, he dicided to continue his study for Master's degree in Structural Engineering program at Chulalongkorn University. During this period he interest in fracture mechanic hence he decide to do the research under the supervision of Associate Professor Dr. Jaroon Rungamornrat and Dr. Weeraporn Phongtinnaboot.